THE MAGNETIC PROPERTIES OF THE SERIES $R_2V_2O_7$; R = Lu, Yb, Tm

By

© LYNDA SODERHOLM, B.Sc.

A Thesis

Submitted to the School of Graduate Studies

in Partial Fulfilment of the Requirements

for the Degree

Doctor of Philosophy

McMaster University

June 1982

THE MAGNETIC PROPERTIES OF THE SERIES

$R_2V_2O_7$; R = Lu, Yb, Tm

DOCTOR OF PHILOSOPHY
(Chemistry)

MCMASTER UNIVERSITY
Hamilton, Ontario

TITLE: The Structure and Magnetic Properties of the Pyrochlores $R_2V_2O_7$; R = Lu, Yb, Tm

AUTHOR: Lynda Soderholm, B.Sc. (McMaster University)

SUPERVISOR: Professor J.E. Greedan

NUMBER OF PAGES: viii, 121

ABSTRACT

The magnetic behaviour of a series of pyrochlores $R_2V_2O_7$ (R = Lu, Yb, Tm) has been studied. They are all ferromagnetic below 70K, with the exchange interactions between vanadium atoms providing the driving force for the ordering. While the rare-earths, Yb(+3) and Tm(+3), remain paramagnetic down to 4K, an exchange field created by vanadium atoms causes the rare-earth and vanadium moments to align parallel. This positive exchange coupling is unusual. The low saturation magnetizations of $Yb_2V_2O_7$ and $Tm_2V_2O_7$ have been attributed to the effects, on the rare-earth ions, of the crystalline electric field.

ACKNOWLEDGEMENTS

I wish to express my gratitute to Dr. C.V. Stager. His outstanding scientific insight, along with his continued encouragement and enthusiasm, have proved invaluable contributions to this work.

I also wish to thank my committee, Dr. J. Greedan for suggesting this project and, together with Dr. M.F. Collins and C.J. Lock, for the many fruitful discussions.

The contributions to this work by J.D. Garrett, J. Couper, G. Hewitson, R. Faggiani and W. Scott are gratefully acknowledged. Also the help provided by Drs. T. Birchall, R. Myers, J. Harvey and W. Prestwich was greatly appreciated.

The entertainment and friendships provided by my colleagues in SSC 432, P. Pilon, J. Britten, J.P. Goral, M. Zvagulis, D. Harvey and K. Franklin made my stay here enjoyable.

Also I wish to acknowledge the superlative typing skills demonstrated by H. Kennelly during the preparation of this thesis.

The financial support of the Natural Sciences and Engineering Research Council of Canada, the Ontario Graduate Scholarship fund, the Chemistry Department and McMaster University are all gratefully acknowledged.

And finally, I wish to thank my family for things too numerous to mention.

TABLE OF CONTENTS

LIST OF FIGURES

CHAPTER 1

INTRODUCTION

Ferromagnetic compounds exist, but they are not common. Compounds which are simultaneously ferromagnetic and semiconducting represent an even more exclusive class, as demonstrated by Table 1-1. There have been many attempts to understand the behaviour of this unusual group of materials since EuO was established as its founding member [Matthias et al., 1961]. It was the rarity of this type of behaviour that first called attention to a report in the literature that a new series of oxides had been synthesized which fell into this category [Bazuev et al., 1976]. A later report supported this finding [Shin-ike et al., 1977]. However, there were only limited preparative techniques, and no chemical analyses, reported in either case. Furthermore there were large discrepancies in the lattice constants, determined by the two groups, for all three compounds. Since both magnetic and electric properties are sensitive to chemical composition, Greedan realized the necessity for well characterized materials. He reported detailed synthetic procedures, along with chemical analyses, for the compounds $(RE)_2V_2O_7$ (RE = Lu, Yb, Tm and solid solutions (Sc_xLu_{1-x}) and (Y_xLu_{1-x})) [Greedan, 1979]. It was the clarification of these synthetic problems which permitted this detailed

Table 1-1

Some Ionic Ferromagnets

Compound	T_c(K)	
EuO*	69	Matthias et al. 1961
$CrBr_3$	33	Tsubokawa, 1960
A_2CuF_2 (K_2CuF_4)	6.3	Yamada, 1974
A_2CrX_4 ($CdCrSe_4$*)	130	Lehmann, 1967
MRh_4B_4 (M = Gd → Ho)	<5	Fertig et al., 1977
$Tb(OH)_3$	3.7	Catanese et al., 1973
$GdCl_3$	2.2	Wolf et al., 1961
$LiTbF_4$	2.8	Guggenheim, 1973
$Tl_2Mn_2O_7$*	117	Fujiwaka et al., 1980
$YTiO_3$*	29	Johnston, 1975
EuS*	16.3	McGuire et al., 1962
Eu_2SiO_4	7.	McGuire and Shafer, 1964
CrO_2	427	Michel et al., 1951
$AMnF_6$ (A = Ni, Zn, Cd)	8-39	Lorin et al., 1981

* also semiconductors

examination of the magnetic properties of this series of vanadium pyrochlores.

General Outline

The organization of this thesis is, perhaps, slightly unusual. It is composed of nine chapters, each organized as an independent unit, with its own introduction, including any theory necessary to understand the concepts presented, followed by data treatment and a discussion of the results. This chapter includes a short outline of the basic theories of magnetism which are used throughout the course of this work.

After presenting an outline of the experimental procedures which were used in this study, and a discussion of the crystal structures of these materials, the basic problem in interpretation of magnetic data is presented in Chapter 4. Chapters 5 and 6 deal with the elucidation of this problem while in Chapter 7 an attempt to reproduce the data, using basic crystal field calculations, is outlined. Chapter 8 includes a discussion of some Mössbauer data and their contribution to the understanding of these pyrochlores.

Basic Theory of Magnetism

The basic magnetic theory needed to interpret the data presented in this thesis is now outlined. The magnitude of the projection, along the field direction of the magnetic moment of an atom in the n^{th} quantum state is given by [Ashcroft and Mermin, 1976]

$$\mu_n = - \frac{\partial E_n}{\partial H} . \qquad (1\text{-}1)$$

The moment at a particular site can be determined by summing over the various energy levels available

$$\langle \mu \rangle = \frac{\sum_n \mu_n \exp(-E_n/kT)}{\sum_n \exp(-E_n/kT)} . \qquad (1\text{-}2)$$

The bulk magnetization for a sample with N_0 identical magnetic atoms per mole is

$$M = N_0 \langle \mu \rangle . \qquad (1\text{-}3)$$

This quantity, M, will be referred to as the saturation magnetization.

To investigate a series of non-interacting spins and their interaction with a field, it is useful to expand the energy in powers of the field

$$E_n = E_n^0 + E_n^{(1)} H + E_n^{(2)} H^2 \ldots\ldots . \qquad (1\text{-}4)$$

Using Eq. (1-1), and terminating this expansion at the second order term yields

$$\mu_n = - \frac{\partial E}{\partial H} = - E_n^{(1)} - 2E_n^{(2)} H . \qquad (1\text{-}5)$$

If this expansion is then substituted into Eq. (1-2), assuming any splitting of energy levels results from the first-order term (Zeeman splitting) is << kT, the exponential may be simpli-

fied since $\exp(-x) \simeq (1-x+x^2/2!)$ if x is small. The exponential becomes

$$\exp(-\frac{E_n}{kT}) \simeq \exp(-\frac{E_n^{(0)}}{kT})[1-\frac{E_n^{(1)}H}{kT}+\frac{E_n^{(1)^2}H^2}{2k^2T^2}][1-\frac{E_n^{(2)}H^2}{kT}] \quad . \quad (1\text{-}6]$$

Substituting Eqs. (1-5) and (1-6) into Eq. (1-2), without assuming that the moment is projected along the field direction, but can take discrete orientations with respect to the field, yields

$$<\mu_j> = [\sum_m \sum_n [-E_n^{(1)}-2E_n^{(2)}H_m][\exp(-E_n^{(0)}/kT)][1-\frac{E_n^{(1)}H_m}{kT}+$$

$$+\frac{E_n^{(1)^2}H_m}{2k^2T^2}][1-\frac{E_n^{(2)}H_m^2}{kT}]] \Big/ \sum_m \sum_n \exp(\frac{E_n^{(0)}}{kT})][1-\frac{E_n^{(1)}H_m}{kT}+$$

$$+\frac{E_n^{(2)}H_m^2}{kT}][1-\frac{E_n^{(2)}H_m^2}{kT}] \qquad (1\text{-}7)$$

where j and m represent the magnetization and field directions respectively. For fields normally attainable in the laboratory, it is possible to ignore the second order terms when simplifying this expression. Also, for dilute, non-interacting systems, it must be true that

$$<u_j> \neq 0 \quad \text{as} \quad H \to 0$$

therefore

$$\sum_n E_n^{(1)} \exp(-\frac{E_n^{(0)}}{kT}) = 0$$

Eq. (1-7) becomes [Mabbs and Machin, 1973]

$$\langle \mu_j \rangle = \frac{\sum_m H_m \sum_n \left[\frac{E_n^{(1)^2}}{kT} - 2E_n^{(2)}\right] \exp\left(-\frac{E_n^{(0)}}{kT}\right)}{\sum_n \exp\left(-\frac{E_n^{(0)}}{kT}\right)} \qquad (1\text{-}8)$$

Since the effect of a magnetic field on the energy levels of an atom is usually small, the E_n's may be calculated using perturbation theory. The Hamiltonian is given by

$$(\hat{H} - \underline{\mu}\cdot\underline{H})|n\rangle = E_n|n \qquad (1\text{-}9)$$

where $\hat{H}$ is the Hamiltonian for the system in the absence of a magnetic field and includes electron-electron repulsion, spin-orbit coupling, and crystal field effects. $-\underline{\mu}\cdot\underline{H}$ is the interaction energy of the moment with a field. The states $|n\rangle$ are the eigenfunctions of the system in the absence of a field and the E_n^0's in Eq. (1-8) are the energies of these unperturbed states. The first order terms, $E_n^{(1)^2}$, are diagonal elements

$$\langle n|\hat{\mu}_j|n\rangle\langle n|\hat{\mu}_m|n\rangle \qquad (1\text{-}10)$$

and indicate how the states change energy in the presence of a magnetic field. These elements are temperature dependent and are known as the Zeeman terms. The second order, off diagonal elements, $E_n^{(2)}$, are given by

$$\sum_{\ell} \frac{\langle n|\hat{\mu}_m|\ell\rangle\langle\ell|\hat{\mu}_j|n\rangle}{E_n^0 - E_\ell^0} \qquad (1\text{-}11)$$

where $\ell \neq n$.

Eq. (1-8) has the form

$$\langle \mu_j \rangle = \sum_m \chi_{jm} H_m \qquad (1\text{-}12)$$

where χ_{jm} is the susceptibility. The macroscopic response to the application of a field can be obtained by summing over all the sites available in the crystal, and has the isotropic form

$$M_j = \chi H_j \qquad (1\text{-}13)$$

where

$$\chi = \frac{1}{3} N_0 \sum_{nn} \chi_{nn} \qquad (1\text{-}14)$$

for a polycrystalline sample. Now the susceptibility is given by

$$\chi = \frac{N_0}{3kTZ} \sum_n [E_n^{(1)2} - 2E_n^{(2)}kT] \exp(-\frac{E_n^{(0)}}{kT}) \qquad (1\text{-}15)$$

with $$Z = \sum_n \exp(-\frac{E_n^{(0)}}{kT}) .$$

It should be noted that the actual definition of the susceptibility is [Ashcroft and Mermin, 1976]

$$\chi = \frac{\partial M}{\partial H} \qquad (1\text{-}16)$$

but when the energy expansion, eq. (1-4), was truncated at the second order term, it was assumed that M was rectilinear in H for

attainable field strengths.

If, in zero field, there is only one energy level, and it is degenerate, Eq. (1-15) reduces to [Mabbs and Machin, 1973]

$$\chi = \frac{N_0}{3p} \sum_n \frac{E_n^{(1)^2}}{kT} \qquad (1\text{-}17)$$

where p is the degeneracy of the level. Since $\Sigma\, E_n^{(1)^2}$ is a constant, eq. (1-17) reduces to the famous Curie Law [Mabbs and Machin, 1973]

$$\chi = \frac{C}{T} \qquad (1\text{-}18)$$

where C is the Curie constant and is given by the following expression

$$C = \frac{Ng_J^2\mu_B^2 J(J+1)}{3k} \qquad (1\text{-}19)$$

This is often written [Cullity, 1972]

$$C = \frac{N(\mu_{eff})^2}{3k} \qquad (1\text{-}20)$$

where μ_{eff} is the effective moment,

$$\mu_{eff} = g_J[J(J+1)]^{1/2}\mu_B \qquad (1\text{-}21)$$

The effective moment should not be confused with the saturation moment

$$\mu_{sat} = g\langle J_z\rangle\mu_B \qquad (1\text{-}22)$$

which is obtained from Eq. (1-3).

Sometimes it is not possible to ignore interactions between spins, and then it is necessary to modify Eq. (1-18) to include these interactions. Weiss [1907] was able to show that deviations from the Curie Law could be understood in terms of an effective field. According to Weiss, the magnetic field felt by the atom is not merely the external field, as was the case for non-interacting systems, but is modified by an internal field. This field, called the molecular field, is proportional to the crystal magnetization

$$\underline{H}_{mf} = \lambda \underline{M} \tag{1-23}$$

where λ is the molecular field constant and is temperature independent. The field felt by the atom is now given by

$$\underline{H}_{eff} = \lambda \underline{M} + \underline{H}_0 \tag{1-24}$$

where $\underline{H}_0$ is the external field. The magnetization, Eq. (1-13), is then modified to

$$\begin{aligned} \underline{M} &= \chi(\underline{H}_{mf} + H_0) \\ &= \frac{C}{T}(\lambda \underline{M} + H_0) \end{aligned} \tag{1-25}$$

Rearranging Eq. (1-25) to obtain an expression for the susceptibility yields the Curie-Weiss Law

$$\chi = \frac{C}{T-\theta} \tag{1-26}$$

where θ is the Weiss constant

$$\theta = \lambda C \quad . \tag{1-27}$$

Using Eqs. (1-23) and (1-19), θ may be written

$$\theta = \frac{Ng\mu_B H_{mf}(J+1)}{3k} \quad . \tag{1-28}$$

The hypothesis that H_{mf} is proportional to the existing magnetization implies that the molecular field is a cooperative effect. It was Heisenberg [1926] who first realized that the molecular field arose from quantum mechanical exchange interactions involving the Pauli exclusion principle. This effect depends on the overlap of wavefunctions on adjacent atoms and may be represented by [Heisenberg, 1928; Levine, 1974; Sachs, 1963]

$$\hat{H}_{ex} = -2 \sum_{i<j} J_{ij} \underline{S}_i \cdot \underline{S}_j \tag{1-29}$$

where J_{ij} is the exchange constant. $\underline{S}$, the spin quantum number, is used to minimize confusion. Since the overlap of the wavefunctions, and therefore the exchange interactions, decreases rapidly with distance, the summation can be restricted to nearest neighbours. If there are Z nearest neighbours, and the spins are all the same and lie parallel, the energy of the exchange is given by

$$E_{ex} = -Z(2J_{ex}S^2) \quad . \tag{1-30}$$

This energy is equivalent to the energy of an atom in a molecular field

$$E_{pot} = - S_z H_{mf} \quad . \qquad (1\text{-}31)$$

Equating eqs. (1-30) and (1-31) and using Eq. (1-28), the exchange integral can be related to the Weiss constant [Cullity, 1972]

$$J_{ex} = \frac{3k\theta}{2ZS(S+1)} \quad . \qquad (1\text{-}32)$$

Using this proportionality, it should be possible to obtain some information about the exchange interactions from θ. The susceptibility data may obey the Curie-Weiss Law, however, while the assumptions necessary to obtain eq. (1-31) are not fulfilled. Such a case may occur, for example, when the presence of low lying crystal field states modify the magnetic behaviour. Therefore caution is advised when attempting to interpret θ quantitatively, to insure that the summation over nearest neighbours, as well as absence of low lying crystal field states, are both valid assumptions to make for the case of interest.

The exchange effects discussed here have been developed for nearest neighbour interactions. However, in the case of most oxides, superexchange pathways (see Chapter 5) are often involved since the magnetic ions are too far apart to allow direct overlap of their wavefunctions. However the basic arguments outlined here still apply.

CHAPTER 2

EXPERIMENTAL PROCEDURES

Sample Preparation

The samples were prepared following the procedure outlined by Greedan [1979]. The basic reaction used for all preparations was

$$(RE)_2O_3 + V_2O_5 \xrightarrow[CO/CO_2]{1400°C} (RE)_2V_2O_7 + \frac{1}{2} O_2 .$$

99.99% $(RE)_2O_3$ (Research Chemicals) was fired overnight at 800°C before weighing and combined with reagent grade V_2O_5 (British Drug Houses). Pellets were pressed and then heated in a SiC furnace with temperature control provided by Research Inc. Thermac and Datatrak equipment. The heating schedule was as follows: room temperature to 1400°C in 6 hours, 1400°C for 12 hours, and cool down to room temperature in 6 hours. A reducing atmosphere was obtained by introducing CO_2 and 50% CO/CO_2 (Matheson) into a gas mixing manifold at controlled flow rates. The oxygen partial pressures were controlled in this manner.

Sample Characterization

Sample characterization has been outlined by Greedan [1979]. Total vanadium was determined by atomic absorption and vanadium (+4) content was determined by thermal gravimetric analysis. The absence of impurity phases was checked by X-ray powder diffraction. The data were collected on a Philips diffractometer with a high purity Si (99.999%) internal standard.

Mössbauer

The main components of the Mössbauer apparatus were the source, absorber, cryostat, velocity transducer, waveform generator and synchronizer, calibration system, single and multichannel analyser, detection system and print-out facilities.

The gamma ray source used was ^{170}Tm in $TmAl_2$. The source was made by arcmelting stoichiometric amounts of distilled ^{169}Thulium metal, supplied by Research Chemicals, and 99.999% Aluminum. The reaction was done under half an atmosphere of Argon. An X-ray powder diffraction pattern of the resulting compound agreed with the reported pattern for $TmAl_2$ [Jones et al. 1963]. 0.1 g of $TmAl_2$ was mixed with an equal weight of reactor grade graphite. A pellet was pressed and sealed in a 6061-Aluminum holder under pressure. The holder was then irradiated in the McMaster University Nuclear

Reactor in position 5C for 24 hours with the reactor operating at 2 MW. The neutron flux at position 5C was about 1.4×10^{13} neutrons sec^{-1} cm^{-2}. The theoretical gamma ray activity of the source was 195 mC but the gamma ray flux at a distance of 0.25 meters was indicative of a source activity of about 100 mC. The decay scheme is shown in Fig. 2-1.

The source, and in some spectra the sample, were maintained at a temperature of 4K in a detachable tail research cryostat manufactured by Janis Research Company. The temperature was determined using a calibrated Allen-Bradley 47 ohm, 1/4 watt carbon resistor coupled to a Cryogenic Research Company temperature controller. The liquid helium boil-off rate was 200 - 300 ml/hour.

For spectra obtained at 77K the samples were placed in an Air Products and Chemicals Model OC-20 Cryo-Tip while the source remained at 4K in the cryostat. The temperature was controlled with a platinum resistor in a control circuit. An accurate temperature reading was obtained from a calibrated chromel versus gold - 0.07 atom % Fe thermocouple.

The Mössbauer experiment involved imparting a Doppler velocity to the source relative to the sample. This was accomplished using an Elscint Transducer in conjunction with an Elscint Model MFD-4 Mössbauer Function Generator and Driving Unit. The transducer moved in a symmetric sawtooth waveform which resulted in a constant acceleration motion. The sense

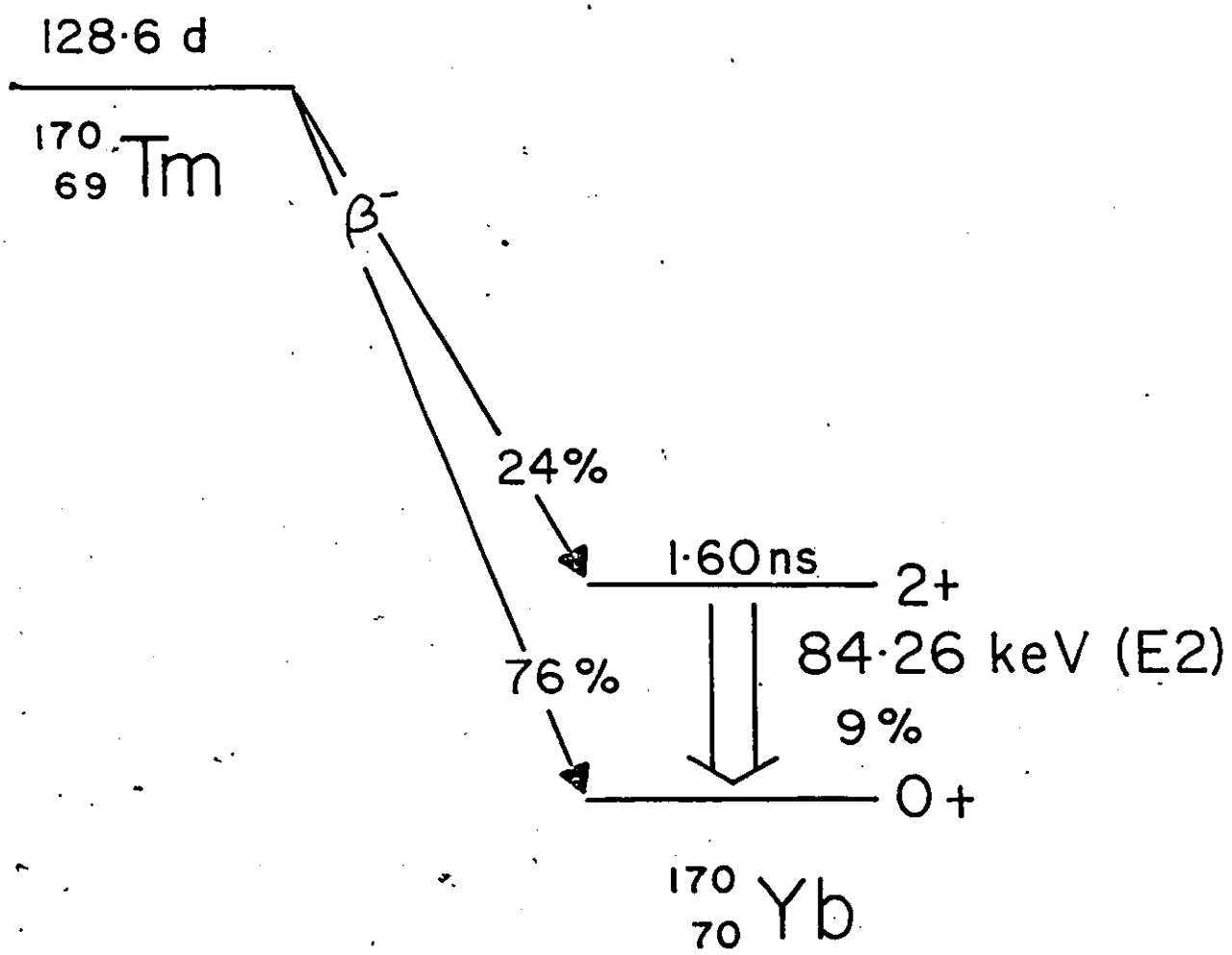

Figure 2-1 The decay scheme of $^{170}_{70}Yb$.

of the transducer was controlled by a Northern-900 series multichannel analyser which was operated in the multiscaling mode. The drive velocity was calibrated using an iron-foil sample on the opposite end of the transducer. The source was ^{57}Co in Pd supplied by New England Nuclear Corporation.

The $TmAl_2$ source was attached to a stiff 90 cm long aluminum rod in the cryostat such that the source to detector distance was about 30 cm. The transmitted gamma radiation was detected by a Harshaw NaI(Tl) crystal 2 mm thick matched to a photomultiplier tube. A tin filter 0.08 cm thick was placed over the detector to filter out about 90% of the 52 keV X-rays while permitting 50% of the 84 keV gamma rays to pass through.

The appropriate 84 keV line was selected by adjusting the upper and lower voltages on the single channel analyser. The data were accumulated and stored in the multichannel analyser in either 512 channels with no folding or 256 channels with automatic folding of the triangular waveform. The data were then transferred onto a teletypewriter and paper tape punch T/T33. Finally the data were transferred to the computer for processing.

Neutron Diffraction

The neutron powder diffraction data were collected at the McMaster Nuclear Reactor using a triple axis spectrometer

operating in the double axis mode. Details of the apparatus may be found in Rowe [1966]. The neutron wavelength of 1.4 A was selected from the 200 reflection of a copper single crystal. The wavelength, zero angle and peak widths were obtained from fitting copper powder data.

Approximately seven grams of finely powdered sample were placed in a cylindrical vanadium holder with a diameter of 7 mm, except in the case of $Lu_2V_2O_7$ where approximately 1.5 grams were placed in a 3 mm. sample holder.

Intensities were normally measured at room temperature. For $Yb_2V_2O_7$ measurements were made at 100K. These temperatures were obtained using an Air Products and Chemicals Inc. Displex Closed-Cycle Refrigeration System and maintained using an Air Products Model APB-B Temperature Controller. Temperatures were measured using a calibrated chromel versus gold - 0.07 atom % Fe thermocouple.

Magnetization Measurements

A pellet of the finely powdered sample was pressed and weighted. The pellet was attached to the end of a 4 mm quartz rod with either GE 7031 varnish or Sauereisen Cement Company ceramic cement.

Data were collected using a Princeton Applied Research vibrating sample magnetometer Model FM-1 with a Magnion water-cooled electromagnet. The system was controlled by and data

collected on a Texas Instruments on-line mini-computer. The magnet was calibrated using a 0.07507 g pure nickel standard with a calibration constant of 58.6±0.1 emu g^{-1} [Crangle and Goodman, 1971] at 4K. Temperatures in the range 4 - 300K were maintained using an Andonian Associates cryostat in conjunction with a Temperature Control System. Temperatures were measured using a calibrated chromel versus gold - 0.07 atom %. Fe thermocouple.

The susceptibility data on the solid solutions $(Sc_xLu_{1-x})_2V_2O_7$, $(Y_xLu_{1-x})_2V_2O_7$ and $Lu_2V_2O_7$ were collected using the Faraday method because their magnetic signals were too small to be measured by the method outlined above. These data were supplied courtesy of Dr. A.P.B. Lever at York University.

CHAPTER 3

ATOMIC STRUCTURES

Introduction

The pyrochlore structure is typified by the mineral pyrochlorite, $CaNa(Nb,Ta)_2O_6F_6$. It can be thought of as intermediate between the fluorite, CaF_2, and C-type rare-earth, C-RE_2O_3, structures.

CaF_2 crystallizes in the Fm3m space group [Bragg, 1914] and may be regarded as a cubic close-packed Ca^{+2} lattice with all the tetrahedral holes occupied by F^-. The site symmetry of Ca^{+2} is m3m. On the other hand C-RE_2O_3, typified by Y_2O_3, crystallizes in the cubic space group Ia3 [Paton and Malsen, 1965]. There are two different crystallographic sites occupied by yttrium, one with $\bar{3}$ and the other with 2 symmetry. Both sites have been described as having either distorted cubic or distorted octahedral coordination [Paton and Malsen, 1965].

The pyrochlore, $A_2B_2O_7$, can be viewed as intermediate between these two structures. Removal of one-eighth of the anions from the fluorite structure, as shown in Fig. 3-1, coupled with the ordering of A and B into two cation sites, results in the pyrochlore structure [McCauley, 1980]. The

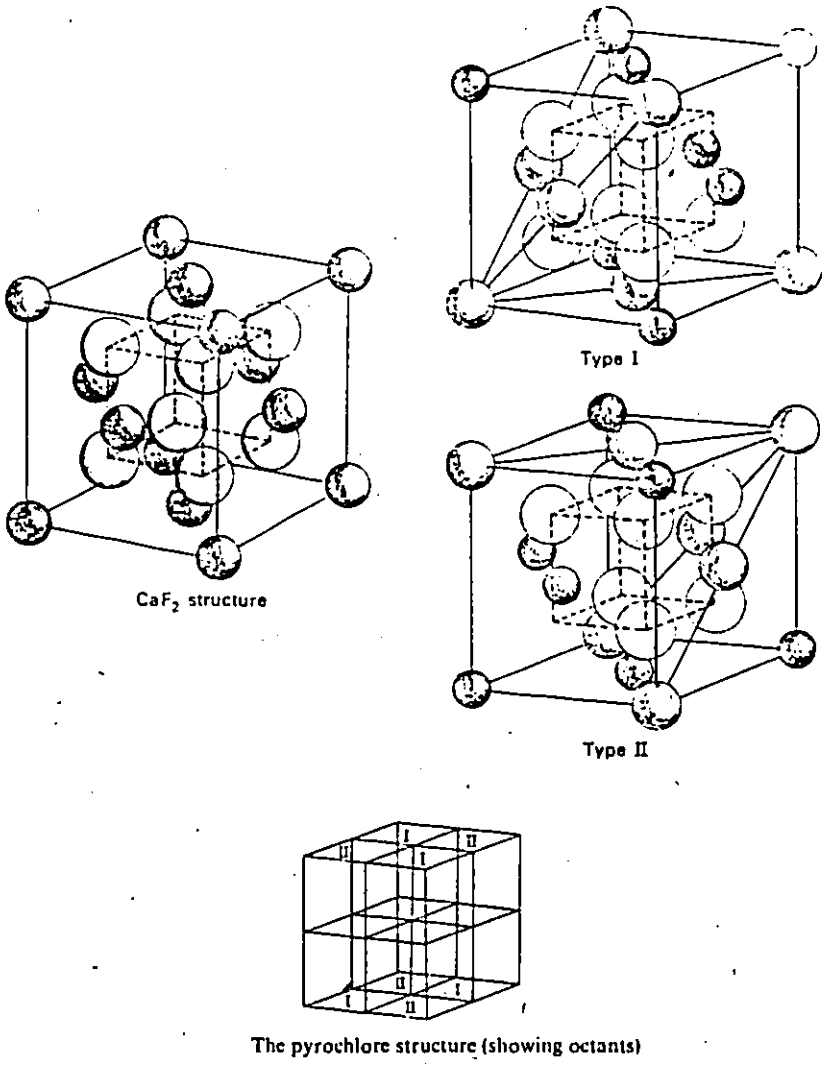

Figure 3-1 The pyrochlore structure can be described by dividing the unit cell into eight octants. There are two types of octants, as shown, each based on the fluorite structure with one anion removed. Taken from Galasso [1970].

removal of more anions, leaving only three-quarters of the tetrahedral sites occupied, along with disordering of the cations over the available positions, results in the C-RE_2O_3 structure.

The pyrochlore structure has Fd3m symmetry. All atoms are on special positions as shown in Table 3-1. The origin was chosen at the centre ($\bar{3}$m) position which is occupied by the A cation. The only variable positional parameter is the x parameter of the oxygen.

The structure may also be viewed as a framework of corner-sharing $(BO_6)^{n-}$ octahedra with the A cations in the interstices [McCauley, 1980]. Therefore there are two different coordination polyhedra within the structure. The larger A atom is 8-fold coordinated with what may be regarded as an equitorial crown of six equidistant oxygen with two axial O(2) atoms at much shorter distances from A. The smaller B cations are surrounded by six equidistant oxygen atoms which form a trigonally distorted octahedron.

The value of the variable oxygen x parameter determines the extent of the distortion of the polyhedra. A value of $x = 0.375$ would result in regular cubes around the A-cation while a value of $x = 0.4375$ would permit regular octahedra about the B cation.

The structure refinements of the three pyrochlores $Lu_2V_2O_7$, $Yb_2V_2O_7$ and $Tm_2V_2O_7$ were undertaken to determine the

Table 3-1

Space group		Fd3m	
		origin at center ($\bar{3}$m)*	
		8 formula units/unit cell	
Positions	Re	16(c)	$\bar{3}$m
	V	16(d)	$\bar{3}$m
	O(1)	48(f)	mm
	O(2)	8(a)	$\bar{4}$3m

*alternate origin at $\frac{1}{8}\ \frac{1}{8}\ \frac{1}{8}$ from $\bar{3}$m at $\bar{4}$3m

variable x parameters of the 48f oxygens. The V-O(1)-V bond angles, which depend on the x parameter, are of interest since the magnetic interactions of the vanadium atoms are postulated to involve this superexchange pathway.

Experimental Section

Precision lattice constants were determined from X-ray powder data using a Philips diffractometer with graphite monochromatized Cu K_α radiation and a Si(99.999%) internal standard. A least squares refinement was performed on 14 - 16 indexed reflections in the range $14° < 2\theta < 90°$.

The atomic structures were determined from neutron data because there is a larger relative contribution from oxygen atoms, to neutron over X-ray scattering. The data were collected on the McMaster triple axis spectrometer operating in the double axis mode. The neutron wavelength of 1.4 A and the zero angle were verified by calibration with copper powder. A single channel detector, with a count time of about 10 min per point, was used to collect the $Yb_2V_2O_7$ and $Tm_2V_2O_7$ data. $Lu_2V_2O_7$ data were collected with a position sensitive detector and a monitor count of about 7×10^6. Data were collected in the range $10° < 2\theta < 115°$.

Powdered samples were placed in a 9 mm cylindrical vanadium sample holder for all three data sets. A check for secondary extinction effects in $Lu_2V_2O_7$ was made with the sample in a 5 mm cylindrical holder. As a check for absorption

the straight-through beam, reduced to the sample size, was counted with the sample in place, without the sample, and without the sample but masked with cadmium.

Values of I_0 for the observed reflections in the three structures are shown in Table 3-2.

Data Treatment

The scale, oxygen x-parameter, isotropic RE and O temperature factors were refined from 24 - 25 integrated intensities using the powder refinement program MARYSE [L'Helgoulach, 1975]. The program does a full matrix least square refinement which minimizes the function $\sum_{k=1}^{r} \omega_k (|F_0|_k^2 - |F_c|_k^2)^2$. The weighting scheme chosen was $\omega = 1/\sigma_k^2$ where

$$\sigma_k = \sqrt{I_k^{bkg} + I_k^{tot}} .$$

Experimental determination of the absorption by the sample showed $\mu R < 2$ in all three pyrochlores, therefore no absorption corrections were applied [Kasper and Longsdale, 1959]. A comparison of I_{440}/I_{531} from $Lu_2V_2O_7$ data obtained in a 5 mm to a 9 mm sample holder showed no significant change in the intensity ratio, therefore no corrections for secondary extinction were made. Lorentz corrections were made by the program. Scattering lengths were taken from Bacon [1977].

Table 3-2

Fo^2 and Fc^2 for $Lu_2V_2O_7$, $Yb_2V_2O_7$ and $Tm_2V_2O_7$

	$Lu_2V_2O_7$		$Yb_2V_2O_7$		$Tm_2V_2O_7$	
	Fo^2	Fc^2	Fo^2	Fc^2	Fo^2	Fc^2
111	13.3	13.5	98.0	87.4	12.1	11.5
311/222	140.4	176.7	717.7	775.0	118.4	159.9
400	245.2	161.8	101.5	32.1	244.1	156.6
331	1024.1	863.5	2115.6	1857.7	1034.1	813.2
422	153.3	144.9	248.3	196.4	151.0	138.3
511/333	701.8	605.8	1290.9	1210.1	573.8	571.3
440	1842.5	1864.4	3561.7	3743.3	1540.7	1671.6
531	248.	185.6	892.0	771.6	202.0	160.2
620	180.1	138.3	230.9	212.6	137.2	146.0
533/622	371.2	487.1	1532.9	1790.5	289.1	414.9
444	47.2	20.1	unobs		unobs	
711/551	521.6		1029.2	936.9	456.6	432.5
642	unobs		152.1	34.5	69.0	23.0
731/553	468.5	581.6	871.0	827.9	516.5	542.1
800	695.4	670.0	1390.6	1377.5	637.6	574.7
733	1747.1	1746.6	3047.9	3098.7	1652.6	1562.6
822/660	1108.2	1104.8	1535.8	1492.7	1079.6	1048.2
751/555/662	910.1	988.2	2600.6	2876.8	762.0	809.5
840	unobs		unobs		unobs	
911/753	1041.4	1026.0	2450.7	2324.9	891.6	866.2
664	311.1	304.8	483.3	442.6	265.9	306.8
931	48.9	55.8	397.6	310.8	17.6	24.4
844/931/771/755 10.20/862	2744.8	2768.0	6006.4	5914.3	2232.0	2251.9
951/773 10.22/666	3231.7	3185.1	5569.3	5612.7	2648.9	2684.5
953	unobs		494.4	407.9	unobs	
10.42/11.11/775	649.5	603.0	1069.1	937.1	435.5	560.6
880/11.31/971/955	1924.1	1793.8	4043.4	3772.7	1537.3	1383.3

Discussion

The values obtained for the structural parameters are shown in Table 3-4. The metal-metal and Re-O(2) bond lengths are determined directly from the lattice constants since RE, V and O(2) sit on special positions. All the metal-metal distances are greater than the sum of their crystal radii [Shannon, 1976].

The RE ions are isolated from the B-O(1) network, being strongly bonded only to two O(2) atoms. The RE-O(2) distances are significantly shorter than the sum of the crystal radii while RE-O(1) distances are long and their interaction considered weak. Therefore there is relatively little interaction between the RE and V atoms.

The x-paramaters are the same within experimental error for all three compounds. L.G. Nikiforov [1972], reported a method for estimating this positional parameter in the pyrochlores from a geometric analysis of the ion contacts. He concluded that the x-value could be determined by solving the system of inequalities:

$$\frac{1}{2} - r_0\sqrt{2}/a \geq y \geq 2r_0/a$$

$$\frac{1}{8}(3-\sqrt{3[r_B-r_0)/(r_A+r_0)]^2-2}) \geq y$$

$$\geq \frac{3}{8} - \sqrt{[(r_B+r_0)/a]^2 - \frac{1}{32}}$$

Table 3-4

Selected Bond Distances and Bond Angles in $Lu_2V_2O_7$, $Yb_2V_2O_7$ and $Tm_2V_2O_7$

	$Lu_2V_2O_7$	$Yb_2V_2O_7$	$Tm_2V_2O_7$
b(RE) (10^{-12}cm)	.730	1.26	.720
a_o(8)	9.928(2)	9.945(1)	9.973(1)
x/a O(1)	0.4187(8)	0.4199(8)	0.4197(9)
R(%)	5.84	6.25	7.61
R(weighted)	7.20	6.93	8.12
Bond Lengths			
RE-RE	3.510(3)	3.516(2)	3.526(2)
V-V	3.510(3)	3.516(2)	3.526(2)
RE-O(1)	2.426(2)	2.438(2)	2.445(2)
RE-O(2)	2.149(3)	2.153(2)	2.159(2)
RE-O(sum of ionic radii)	2.357	2.365	2.374
V-O(1)	1.931(3)	1.930(3)	1.936(4)
V-O(2)	4.116(3)	4.123(2)	4.135(2)
Bond Angles			
O(1)-V-O(1)	82.9(10)	83.2(10)	83.2(10)
O(1)-V-O(1)	97.1(10)	96.8(10)	96.8(10)
V-O(1)-V	130.6(10)	131.3(10)	131.1(10)
O(1)-RE-O(1)	105.2(10)	105.1(10)	105.1(10)
O(1)-RE-O(1)	74.8(10)	74.9(10)	74.9(10)
O(2)-RE-O(2)	180.	180.	180.

r_0, r_A, r_B represent crystal radii and $y = x-0.125$. The application of this method to the series under investigation resulted in the values found in Table 3-5. The calculated x-parameters are in agreement with those obtained experimentally but the errors are much larger.

The O(1) x-parameters are considered important because they determine the environment of the vanadium atoms. Later it will be argued that it is the vanadium ions, interacting through intermediate oxygen atoms that are responsible for magnetic ordering in these materials. Therefore it should be emphasized that the x values are the same, within experimental error, for all three pyrochlores. They are also in the range of x-values found for other compounds with the pyrochlore structure, as shown in Table 3-6.

Table 3-5

A comparison of calculated [Nikiforov, 1972] to experimental values for the O(1) x-parameter

	$Lu_2V_2O_7$	$Yb_2V_2O_7$	$Tm_2V_2O_7$
x (calc)*	.427(18)	.427(19)	.428(18)
x (exp)	.4188(8)	.4199(8)	.4197(9)

*crystal radii from Shannon [1976]

Table 3-6

A comparison of the O(1) x-parameter and the M-O-M bond angles in some $A_2M_2O_7$ pyrochlores

Compound	X-O(1)	M-O-M	Ref
$Er_2Ti_2O_7$	.4200(11)	131.3(6)	Knop et al. 1965
$Y_2Sn_2O_7$	.4120(9)	127.1(4)	Knop et al. 1968
$Sm_2Sn_2O_7$	.4167(26)	129.5(14)	Knop et al. 1968
$La_2Sn_2O_7$	.4216(10)	132.2(6)	Knop et al. 1968
$Sm_2Ti_2O_7$	.4259(20)	134.5(11)	Knop et al. 1969
$Gd_2Ti_2O_7$	.4271(19)	135.2(10)	Knop et al. 1969
$Y_2Ti_2O_7$	.4218(7)	132.3(4)	Knop et al. 1969
$Lu_2Ti_2O_7$	.4221(16)	132.4(9)	Knop et al. 1969

CHAPTER 4

MAGNETIC PROPERTIES

Introduction

This chapter is divided into three sections. The first reviews the magnetic data, already present in the literature, which sparked initial interest in these compounds. Following this there is an outline of the methods used to treat the data obtained in this study. The final section deals with the interpretation of these results.

The preparation, along with magnetic and electrical properties of the rare-earth vanadium pyrochlores were first reported by Bazuev et al. [1976]. Magnetic data on $Lu_2V_2O_7$ between 4K and 300K were consistent with the onset of ferromagnetic ordering of the vanadium (+4) spins at about 80K. Resistivity measurements, done on a sintered pellet, showed an activated transport mechanism interpreted as consistent with semiconducting behavior. Shin-ike et al. [1977] investigating the same series, also found $Lu_2V_2O_7$ to be a ferromagnet with $77K < T_c < 90K$. Their conductivity measurements were also consistent with semiconducting behaviour.

Both groups investigated the magnetic behavior of

$Yb_2V_2O_7$ and $Tm_2V_2O_7$. Unlike $Lu_2V_2O_7$, these compounds have magnetic moments associated with the rare-earth as well as the vanadium ions (see Table 4-1). Bazuev et al. [1976] reported the susceptibility, χ, as a function of temperature for both compounds in the range $77K < T < 300K$. $Tm_2V_2O_7$ data were interpreted in terms of the Curie-Weiss law with constants as shown in Table 4-2. The χ^{-1} versus T curve for $Yb_2V_2O_7$ showed an inflection at 190K, therefore the Curie-Weiss law was used to fit two regions, $77K < T < 190K$ and $190K < T < 300K$, independently. Although no explanation for the inflection was given, the susceptibility data for $Yb_2V_2O_7$, as well as $Tm_2V_2O_7$, were interpreted as consistent with behavior expected from a ferromagnet at $T > T_c$.

Shin-ike et al. [1977] agreed with the basic interpretation of the $Tm_2V_2O_7$ data but could not detect an inflection in their χ^{-1} versus T plot of $Yb_2V_2O_7$ data. The effective moment, obtained from this plot, differed considerably from both of those reported by Bazuev.

Finally, the saturation magnetization, determined at 4K, was reported for $Lu_2V_2O_7$, $Yb_2V_2O_7$ and $Tm_2V_2O_7$ [Bazuev et al. 1977]. The value obtained for $Lu_2V_2O_7$ was near the expected 2.0 μ_B molecule^{-1} for a spin only d^1 system. The saturation moments, μ_{sat}, for both $Yb_2V_2O_7$ and $Tm_2V_2O_7$ were much lower than expected for ferromagnetic coupling between a free ion rare-earth spin and a spin-only vanadium moment.

Table 4-1

Calculated values for magnetic ions used here

	g_J	J	$\mu^*_{sat}(\mu_B)$	μ^{**}_{eff}
Lu(+3)		0	0	0
Yb(+3)	8/7	7/2	4	4.5
Tm(+3)	7/6	6	7	7.56
V(+4)†	2	1/2	1.0	1.73

* $\mu_{sat} = g_J J \mu_B$

** $\mu_{eff} = g_J[J(J+1)]$

† spin only values

Table 4-2

A comparison of susceptibility constants

	Bazuev 1976	Shin-like 1977	Bazuev 1977	This Work	Theoretical†
$Lu_2V_2O_7$					
$\mu_{eff}(\mu_B/molecule)$	2.62	2.76	2.71	2.69	2.45
θ(K)	+100	+76	+100	+83(2)	
$Yb_2V_2O_7$					
$\mu_{eff}(\mu_B/molecule)$	4.24T>190 3.40T<190	6.45	-	-	6.87
θ(K)	+68*T<190 +9*T >190	+11	-	-	
$Tm_2V_2O_7$					
$\mu_{eff}(\mu_B/molecule)$	7.15	10.9	11.05	10.90	10.96
θ(K)	+14	+10	-	-10(2)	

† $\mu_{eff}(theo) = \sqrt{2(\mu_{eff}^2(RE)+\mu_{eff}^2(V))}$

* from graph

Table 4-3

A comparison of saturation moments

μ_{sat} (μ_B/F.U.)

	Bazuev 1976	Shin-ike 1977	Bazuev 1977	This work
$Lu_2V_2O_7$	1.85	-	1.85	1.86(10)
$Yb_2V_2O_7$	-	-	4.70	5.42(10)
$Tm_2V_2O_7$	-	-	1.72*	2.43(10)

* reported 6 wt % $TmVO_3$ impurity

However, all three compounds were classed as ferromagnetic semiconductors, with low values of μ_{sat} attributed to quenching of the rare-earth moments by the crystalline electric field.

The rectilinear dependence of the inverse susceptibility on temperature coupled with a positive Weiss constant, are indicative of ferromagnetic ordering of the vanadium spins below about 80K for $Lu_2V_2O_7$. Furthermore the 4°K saturation magnetization is close to the value expected for parallel alignment of V(+4) spin-only moments. However the data for $Yb_2V_2O_7$ and $Tm_2V_2O_7$ appear more complex. The report of an inflection in the χ^{-1} vs T curve for $Yb_2V_2O_7$ along with low saturation magnetizations for both compounds renders ambiguous the assignment of these compounds as ferromagnets. Since there are so few known examples of ferromagnetic semiconductors, work was undertaken to augment existing results and to clarify the interpretation of the data.

Data Treatment

The critical temperatures were determined by making use of the expression [Arrot, 1957]

$$a(T-T_c)M + bTM^3 = H \qquad (4\text{-}1)$$

in the region of T_c. a and b are constants and H is the applied field corrected for demagnetizing effects. The de-

magnetizing corrections to H were assumed to be negligible since the moment is low in the region of T_c [Maguire, Flanders, 1969]. It should be noted that this equation was derived using molecular field theory and is not supported by modern critical theory, which states that the index of M should be δ where $\delta \approx 4\text{-}5$ [Stanley, 1971]. However, the determination of T_c using Eq. (4-1) is still widely employed.

Magnetization data as a function of field were obtained at several temperatures in the region of T_c. The temperature giving a rectilinear M^3 vs H curve and a zero intercept was interpreted as T_c. An example is shown in Fig. 4-1. Results are shown in Table 4-4.

The saturation moments at 4K were determined by fitting magnetization versus field curves to

$$M(H,T) = M(T)\left[1 - \frac{A}{H}\right] + BH \qquad (4\text{-}2)$$

where A and B are constants. This is an empirical approximation adapted from Brown [Brown, 1941; Morrish, 1966]. Since A was large and B small, M. was obtained by extrapolation to infinite field. M versus H curves at 4K are shown in Fig. 4-2.

Magnetizations as a function of temperature at $T < T_c$, for all three compounds, were constructed by fitting isothermal data for several temperatures to Eq. (4-2) and extrapolating to infinite field. M. Versus T curves obtained by this method are shown in Fig. 4-3.

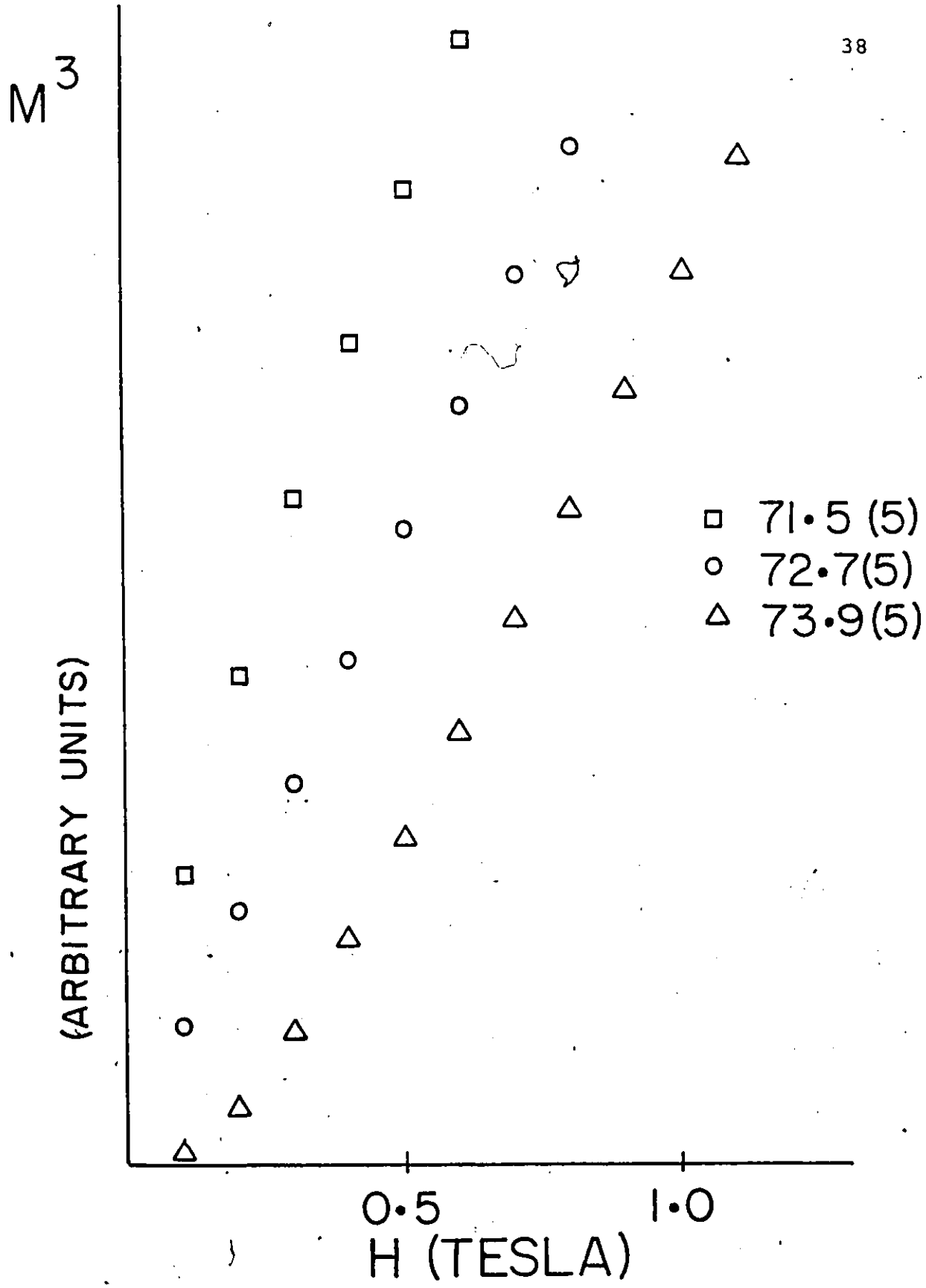

Figure 4-1 The Arrot plot used to determine the critical temperature of $Yb_2V_2O_7$. The temperature of the isotherm which intercepts the origin was interpreted as T_c.

Table 4-4

Critical temperatures for $(RE)_2V_2O_7$; RE + Lu,Yb,Tm

	T_c Bazuev 1976/1977	T_c This work	a_0
$Lu_2V_2O_7$	73.0(5)	74.6(4)	9.928(2)
$Yb_2V_2O_7$	85 - 90	73.2(4)	9.945(1)
$Tm_2V_2O_7$	85 - 90	71.4(2)	9.973(1)

The critical temperatures for the pyrochlores listed along with the cell constant (a_0) to show the trend of decreasing T_c with increasing a_0. Numbers in brackets are the errors in last digit.

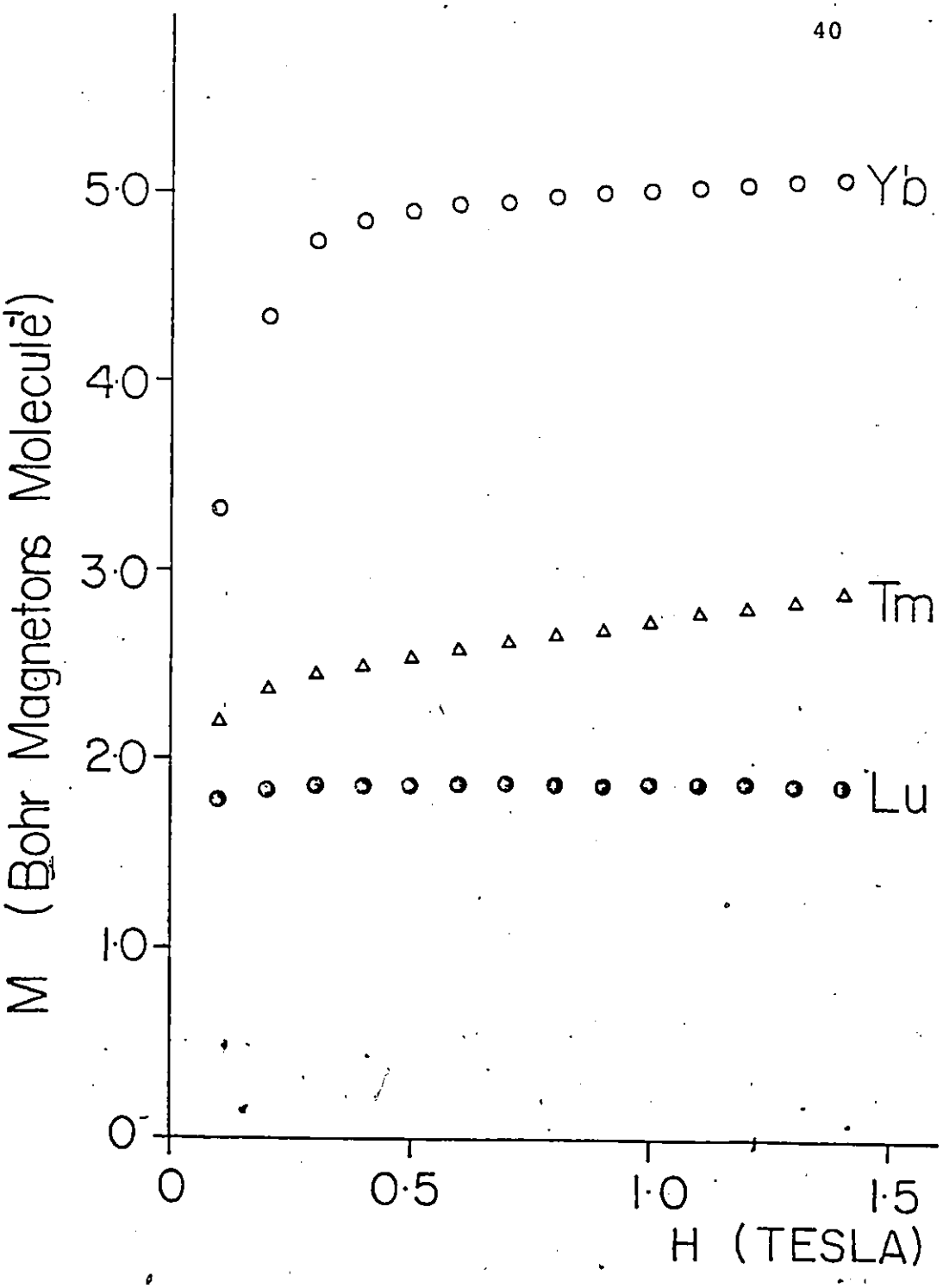

Figure 4-2 Magnetic moment versus field curves for $Lu_2V_2O_7$, $Yb_2V_2O_7$ and $Tm_2V_2O_7$ at 4K.

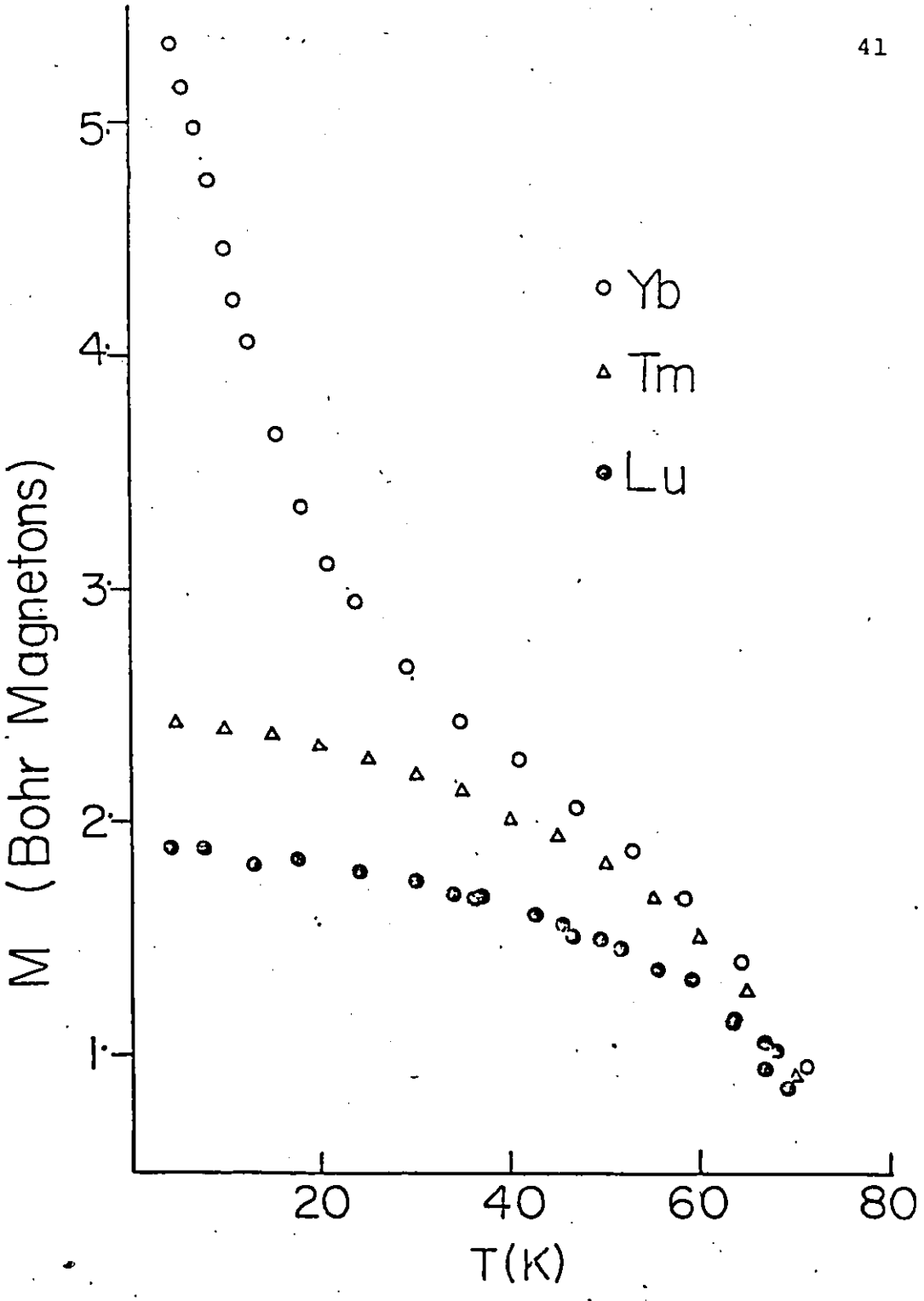

Figure 4-3 Magnetic moment, per $(RE)_2V_2O_7$ molecule, versus temperature curves obtained from M versus H curves.

Susceptibility data as a function of temperature were collected in the range 100K $\leq$ T $\leq$ 300K. Values of μ_{eff} and θ were obtained from rectilinear regions of the χ^{-1} versus T plots. No attempt was made to extract these parameters in the case of $Yb_2V_2O_7$ since no rectilinear region was observed in the temperature range studied. Plots of χ^{-1} vs T are shown in Figs. 4-4 to 4-6.

Discussion

The $Lu_2V_2O_7$ data agree well with those obtained previously. The rapid rise to saturation at 4K with low applied fields is characteristic of a ferromagnet. The saturation moment is close to the value expected for parallel alignment of d^1 spin-only moments. At 74.6K there was a drop in magnetization, which was interpreted as the Curie temperature. The effective moment of 2.69 μ_B/F.U. (1.90 μ_B/V^{+4}) is in good agreement with previous results. However, all values are larger than expected for a spin-only d^1 moment. The spin-only value should represent a theoretical upper limit, since the orbital contribution to the moment is antiparallel to the spin contribution. This problem is discussed more fully in Chapter 5.

The saturation magnetizations obtained for $Yb_2V_2O_7$ and $Tm_2V_2O_7$ are larger than those obtained by Basuev (see Table 4-3). The saturation moment of $Tm_2V_2O_7$ was determined to be 2.43(10) μ_B. This is only slightly higher than the 1.86 μ_B

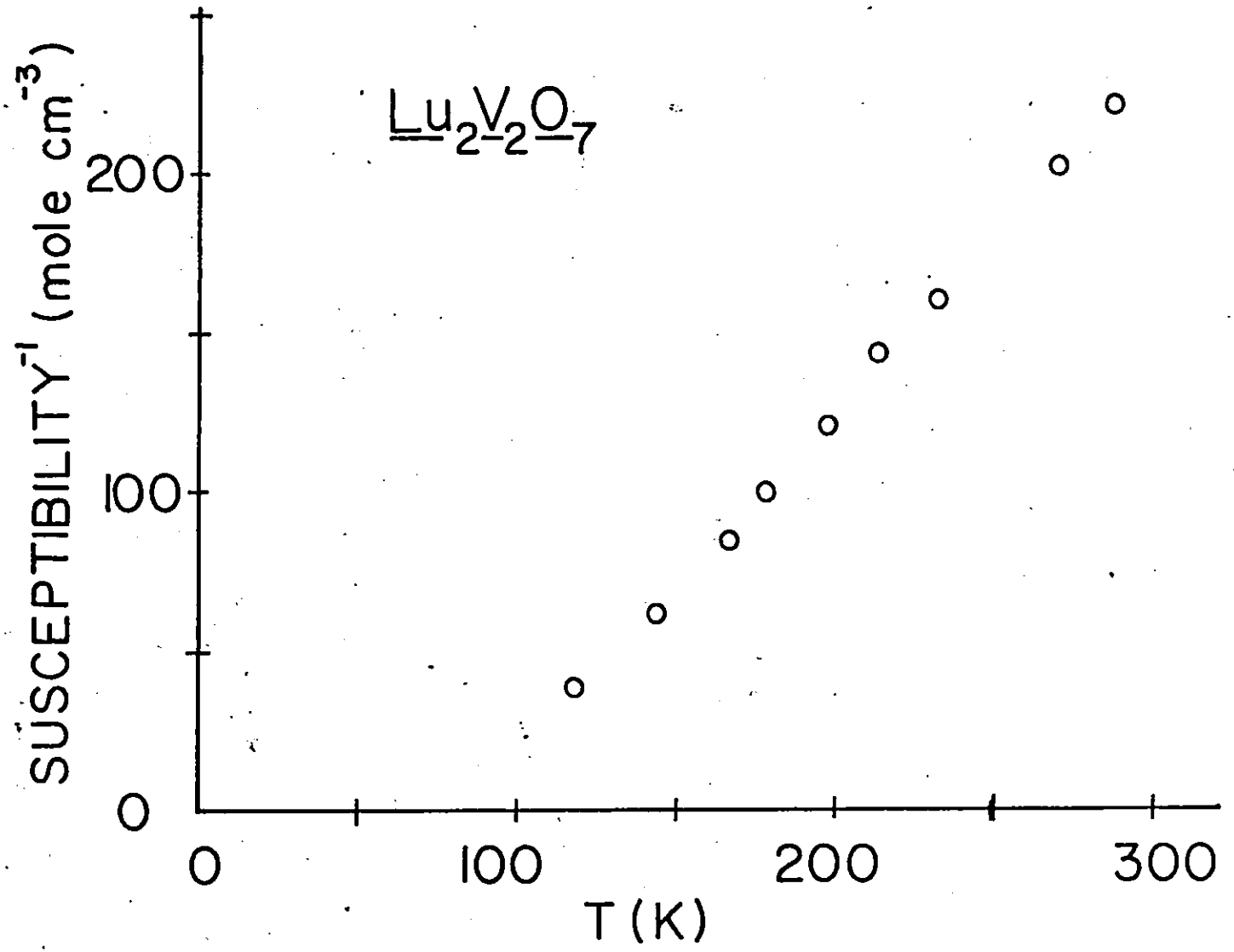

Figure 4-4 A plot of inverse susceptibility versus temperature for $Lu_2V_2O_7$. Data courtesy of A.P.B. Lever, York University.

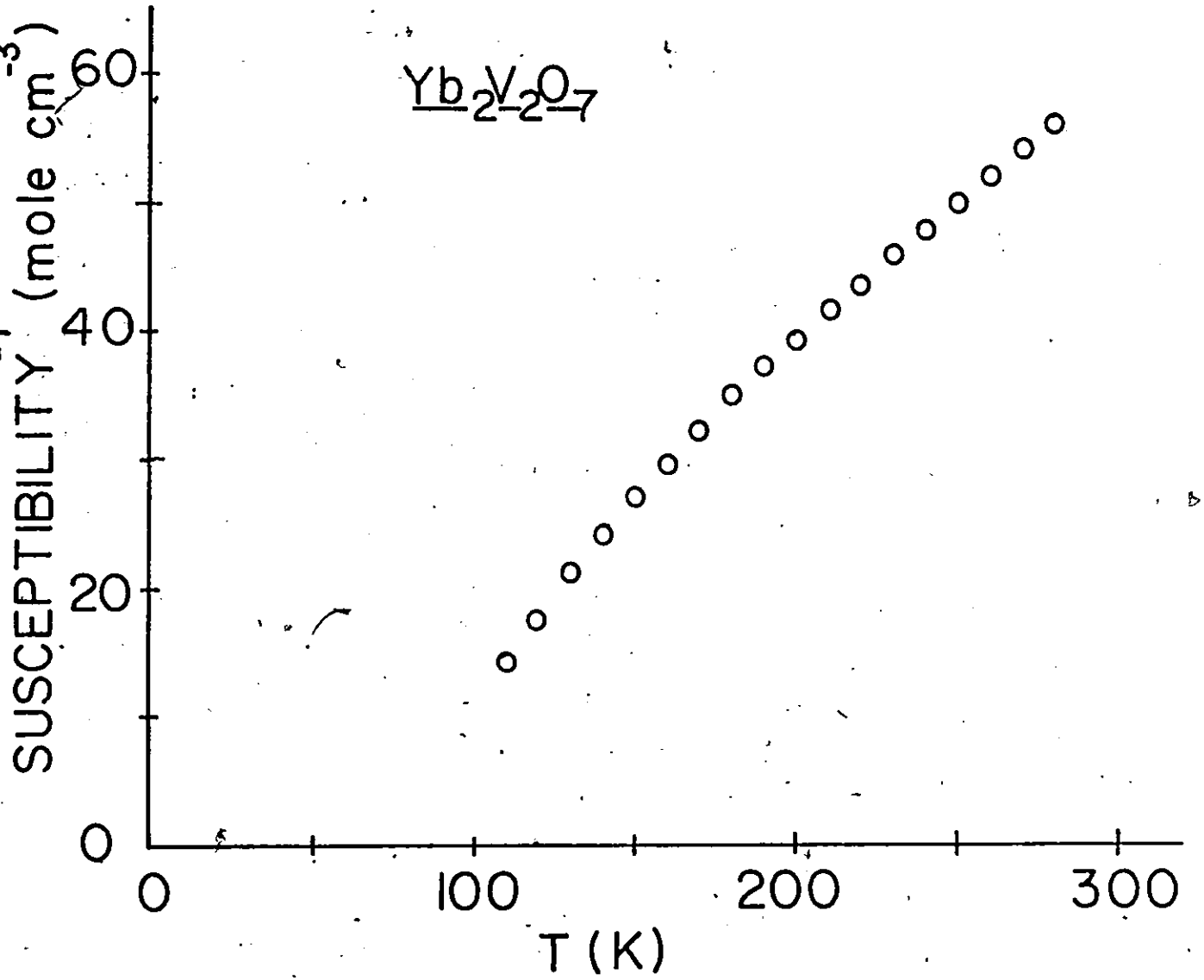

Figure 4-5 A plot of inverse susceptibility versus temperature for $Yb_2V_2O_7$

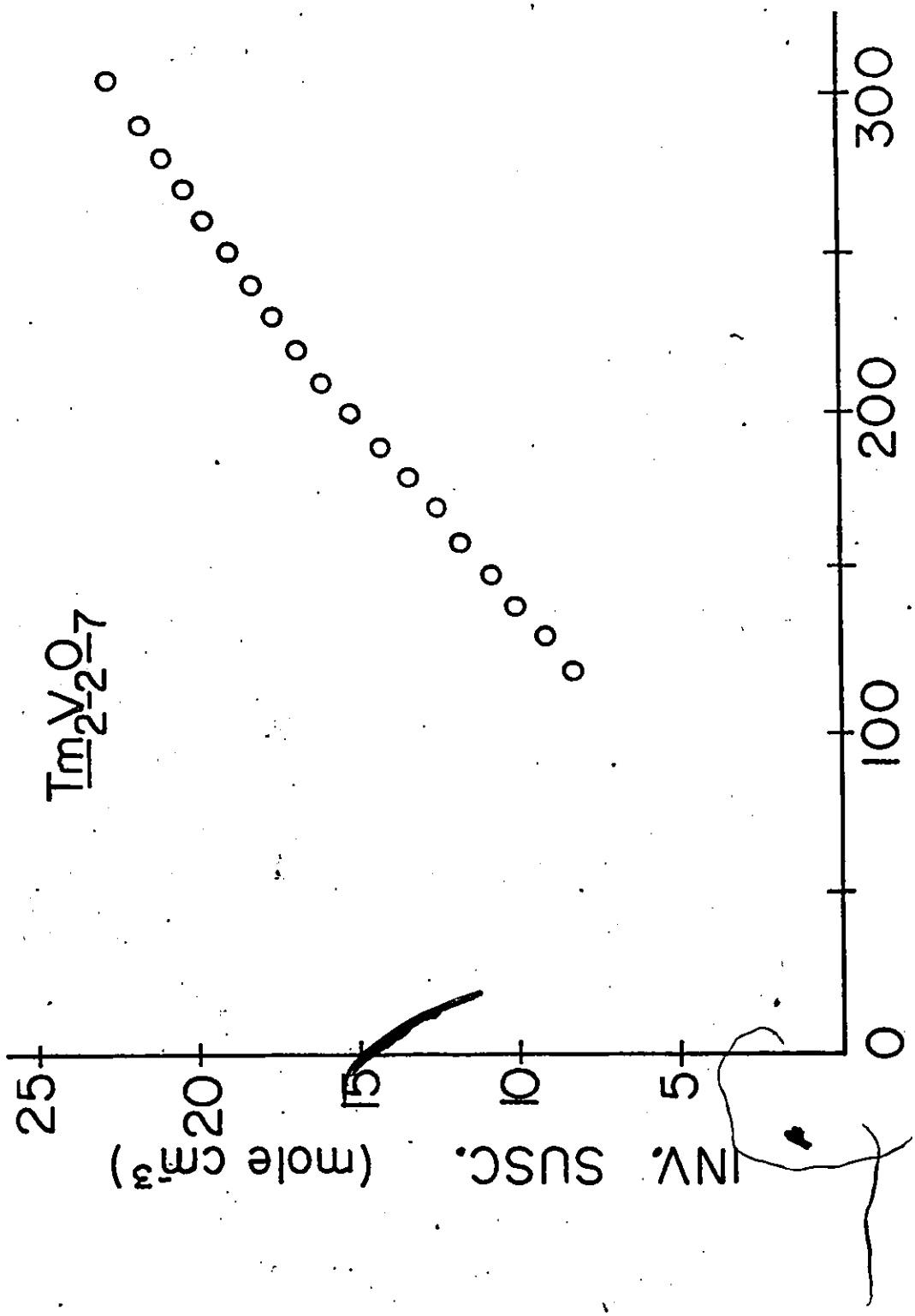

Figure 4-6 A plot of inverse susceptibility versus temperature for $Tm_2V_2O_7$

determined for $Lu_2V_2O_7$, although Tm^{+3} has a free ion g_J^J of 7.0 μ_B. The effective moment, on the other hand, is close to the theoretical value obtained from

$$\mu_{eff} = g[J(J+1)]^{\frac{1}{2}} . \qquad (4-3)$$

The saturation moment of $Yb_2V_2O_7$ is also slightly higher than reported by Bazuev. As previously mentioned, the plot of χ^{-1} versus T exhibited a curvature which did not permit the extraction of Curie-Weiss parameters. However in contrast to the data reported by Bazuev, there was no apparent discontinuity at 190K in the χ^{-1} vs T curve. Furthermore, it is interesting to note the unusual shape of the M vs T curve for $Yb_2V_2O_7$ (see Fig. 4-3). There is a marked decrease in the magnetization at about 35K, well below the reported Curie temperature.

The critical temperatures of all three compounds are very similar and appear independent of the moment on the rare earth ion. However, there is a slight trend to decreasing T_c with increasing cell constant, indicating the dominant interactions are between vanadium atoms, even in the two sublattice systems. This can be explained in terms of the crystal structure. The network of V-O octahedra described in Chapter 3, form a superexchange pathway, allowing interaction of vanadium through intermediary oxygen atoms. The rare-earth atoms, on the other hand, exist as spatially isolated $RE-O_2$

units. Therefore it appears the interactions between vanadium atoms constitute the driving force for magnetic ordering, and these interactions change very little across the series.

If the moments on the vanadium atoms are postulated to order ferromagnetically in $Yb_2V_2O_7$ and $Tm_2V_2O_7$, the low saturation magnetizations must be explained. Assuming free ion gJ values for RE(+3), 0.94 μ_B per V(+4) and parallel coupling, it can be seen from Table 4-5 that there is a large discrepancy between the theoretical and experimental moments. Bazuev attributed the low saturation moments to quenching of the rare earth orbital contribution through the crystal field, pointing out that the moment left after subtracting the vanadium contribution from $Tm_2V_2O_7$ data was very near the spin only value of 1.0 μ_B. This interpretation is unlikely since, for rare-earth ions, spin-orbit coupling is larger than crystal field interactions. This does not mean that the total moment cannot be reduced from a free ion value by interaction with a crystal field. Indeed this is one explanation for the low saturation moments which were obtained for both $Yb_2V_2O_7$ and $Tm_2V_2O_7$.

There is, however, another possibility which should be examined. The rare-earth and vanadium moments may align antiparallel, in which case $Yb_2V_2O_7$ and $Tm_2V_2O_7$ would be ferrimagnetic. This postulate is consistent with the shapes of χ^{-1} versus T curves, which may be considered as the classic

Table 4-5

Predicted saturation moments for some RE-V coupling schemes in bohr magnetons

	Free ion gJ	Ferromagnetic* coupling	Ferrimagnetic** coupling	Expt.
$Yb_2V_2O_7$	4	10	6	5.42
$Tm_2V_2O_7$	7	16	12	2.43

* R↑ V↑ obtained by $2(gJ_{RE}) + 2(\mu_{sat}/V)$

** R↑ V↓ obtained by $2(gJ_{RE}) - 2(\mu_{sat}/V)$

Néel hyperbola expected for a ferrimagnet [Smart, 1966]. The saturation moment calculated using this model fits well for $Yb_2V_2O_7$, as shown in Table 4-5, but the $Tm_2V_2O_7$ moment is lower than predicted, indicating the possibility of an even more complex magnetic structure.

While the ferrimagnetic model for $Yb_2V_2O_7$ appears consistent with both the low saturation magnetization value and the shape of the χ^{-1} versus T curve, it is inconsistent with the shape of the M versus T curve. If the Yb(+3) and V(+4) moments are coupled antiparallel and the initial decrease in magnetization is explained by decoupling of the Yb(3+) moments, there should be a compensation temperature at which the magnetization of the Yb(+3) atoms just cancel that of the vanadium atoms. Such a compensation temperature was not observed.

$Lu_2V_2O_7$ appears to be ferromagnetic, and, according to previous reports, a semiconductor. $Yb_2V_2O_7$ and $Tm_2V_2O_7$, each with two magnetic sublattices, present a more complicated picture. The saturation moments are lower than expected for ferromagnetic coupling and the possibility for other types of coupling may not be ruled out based on magnetic data alone. Indeed, in the case of $Yb_2V_2O_7$, a model involving ferrimagnetic coupling offers itself as a viable alternative. In light of the rarity of ferromagnetic semiconductors, it appears premature to assign $Yb_2V_2O_7$ and $Tm_2V_2O_7$ to this special class.

The next chapter attempts to show that changing the cell constants in these pyrochlores does not drastically alter the magnetic behaviour of the vanadium atoms. The following chapter introduces neutron diffraction data to determine the magnetic structure directly.

CHAPTER 5

SOLID SOLUTIONS

Introduction

It has been postulated that the vanadium atom moments in the pyrochlores $(RE)_2V_2O_7$; RE = Lu, Yb, Tm, are coupled ferromagnetically below about 70K. An investigation of the crystal structures of these compounds indicates that the vanadium-vanadium distance in all three compounds is long. Goodenough [1967] proposed a semiempirical formula to determine the cation separation for localized versus collective electrons in oxides containing first row transition metals.

$$R_c = [3.20-0.5M^+-0.03(Z-Z_{T_i})-0.04S_i(S_i+1)]\text{Å} . \qquad (5\text{-}1)$$

M^+ is the formal valence, $(Z-Z_{T_i})$ the nuclear charge with reference to titanium and S_i is the localized spin. The value of R_c for V(+4) is 2.94 Å. Since the V-V separation is 3.15 Å [Soderholm and Greedan, 1982] in the three pyrochlores there should be no electron delocalization as a result of cation-cation interaction. Therefore, mechanisms for ferromagnetic exchange which rely on delocalized electrons are not appropriate to these compounds.

The most probable pathway for interaction of vanadium spins is a superexchange pathway. For the case of these pyrochlores, the vanadium ion 3d orbitals overlap with the p orbitals of oxygen(1). Although oxygen itself is diamagnetic this mechanism invokes excited state configurations of overlapping V-O-V orbitals [Martin, 1968]. The degree of overlap, as well as the orbitals involved, determine the magnitude and sign of the exchange interaction. Therefore it is possible that small changes in either the cell constant or oxygen x parameter can alter the magnetic behaviour of the vanadium sublattice.

Solid solutions are sometimes used to investigate the effect of changing cell size on magnetic properties. In this chapter the results of such an investigation are discussed in terms of the effect small changes in the lattice constants have on the magnetic behavior of the vanadium atoms in the pyrochlore lattice. The series $(Sc_xLu_{1-x})_2V_2O_7$; $x = 0.1 \rightarrow 0.5$, and $(Y_xLu_{1-x})_2V_2O_7$; $x = 0.2, 0.4$, were studied. Non-magnetic A-type cations were chosen to insure no complications from A-vanadium exchange interactions.

The assumption necessary to the following discussion is that there is a random distribution of the cations on the A-site and that the average cell dimensions are useful as a measure of the behavior on a microscopic scale. In a previous study of the $(Sc_xLu_{1-x})_2V_2O_7$ system [Greedan, 1979] it was noted that the composition $x = 0.4$ and 0.5 were signi-

ficantly reduced, showing the presence of vanadium in an oxidation state lower than +4. It was suggested that this reduced species is vanadium(+3) and its incorporation into the structure led to diminished intensity for the pyrochlore ordering reflections (hkℓ all odd). This is consistent with a disordering of all the cation species among the two sites available in the pyrochlore structure. Both the presence of vanadium(+3) and the cation disorder should have some effect on the magnetic properties.

Data Treatment

Cell constants were determined from X-ray powder data using a Philips diffractometer with graphite monochromized Cu K_α radiation and a Si (99.999%) internal standard. Lattice parameters were obtained from a least squares analysis of 12 - 15 indexed reflections in the range $28° < 2\theta < 90°$. Thermal gravimetric analyses were obtained from Greedan [1979]. The magnetic data were obtained as outlined in Chapter 2.

Saturation magnetizations for the various solid solutions were determined by extrapolation of M vs H curves, obtained at 4K, to zero field. Critical temperatures were obtained from M^3 vs T plots at residual applied fields (0.0045 T). θ_c and c_m values were determined from susceptibility data by a least square fit of 14 - 16 points in range 90K - 300K.

Discussion

The magnetic data for $(Y_xLu_{1-x})_2V_2O_7$, x = .2, .4, and $(Sc_xLu_{1-x})_2V_2O_7$, x = 0 to .5, are shown in Table 5-1. There is little change in magnetic behavior across the series until $(Sc_{.3}Lu_{.7})_2V_2O_7$, after which all measured parameters are seen to change. TGA results, shown in Table 5-2, revealed the incorporation of significant amounts of vanadium(+3) into $(Sc_xLu_{1-x})_2V_2O_7$, x = .4 and .5. Since V(+3) exhibits magnetic properties different from V(+4), the change in magnetic behavior towards the end of the series was attributed directly to the presence of reduced vanadium. As a result, treatment of the magnetic data as a model for the behavior of the vanadium(+4) sublattice in other pyrochlores will be confined to the first part of the series. The data obtained for the compounds $(Sc_xLu_{1-x})_2V_2O_7$, x = .3 to .5, will be treated only in relation to effects on the magnetic behavior of the incorporation of reduced vanadium(+3).

The saturation moments for $(Y_xLu_{1-x})_2V_2O_7$, x = .2, .4, and $(Sc_xLu_{1-x})_2V_2O_7$, x = 0 to .2, are in the range 0.93 μ_B to 1.00 μ_B, as expected for a spin-only d^1 system. The Weiss constants, θ_c's, are relatively similar, although there is some scatter around +85K. These data are all consistent with ferromagnetic ordering and there appears to be little change in the magnetic behavior with change in cell size over the range investigated.

Table 5-1

Summary of the magnetic properties of various $(RE)_2V_2O_7$ solid solution systems

RE	T_c(K)(±1K)	θ_c(K)[a]	C_m(cm^3.mole K)[a]	μ_{eff}/V (μ_B)	μ_{sat}-4.2K (μ_B/V)
$Y_{.40}Lu_{.60}$	71.5	90.2(1),	.91 (1)	1.91(1)	0.98
$Y_{.20}Lu_{.80}$	70	79 (1)	.985(5)	1.96(1)	0.95
Lu	72.5	83.3(6)	.918(7)	1.92(1)	0.93
$Sc_{.10}Lu_{.90}$	69	93.0(5)	.943(7)	1.94(1)	1.00
$Sc_{.20}Lu_{.80}$	67	83.1(4)	.958(4)	1.96(1)	0.93
$Sc_{.30}Lu_{.70}$	56	73.8(8)	1.127(5)	2.12(1)	0.87
$Sc_{.40}Lu_{.60}$	46	62 (2)	1.25 (2)	2.24(2)	b
$Sc_{.50}Lu_{.50}$	36	49 (3)	1.37 (2)	2.34(2)	b

[a] θ_c and C_m were determined from a least squares plot of 14 to 16 data in the range 300K to about 90K. Data may be found in Soderholm and Greedan [1979b]. The numbers in parentheses are the standard deviations in the last significant figure.

[b] Does not saturate in highest field used, 1.5T.

Table 5-2

Experimental and calculated weight gains for solid solutions

	expt.	calc (all V+4)		expt.	calc (all V+4)
$Sc_{.5}Lu_{.5}$	4.95	3.68	$Sc_{.2}Lu_{.8}$	3.13	3.13
$Sc_{.4}Lu_{.6}$	4.31	3.48	$Sc_{.1}Lu_{.9}$	2.96	2.97
$Sc_{.3}Lu_{.7}$	3.33	3.29	$Y_{.2}Lu_{.8}$	3.04	3.02
			$Y_{.4}Lu_{.8}$	3.18	3.23

The effective moments, μ_{eff}, were all larger than the spin-only value of 1.73 μ_B expected for a d^1 system. According to Hund's third rule [Ashcroft and Mermin, 1976], for configurations with less than 1/2 filled shells, the state with lowest energy should have a total angular momentum $J = |L-S|$, therefore the spin only moment should represent an upper limit. A possible explanation of this problem would be the presence of vanadium(+3) in all of the samples since

$$\mu_{eff}V(+4) = 1.73\ \mu_B$$

and

$$\mu_{eff}(V+3) = 2.83\ \mu_B .$$

If the experimental effective moment is considered as

$$\mu_{eff} = \sqrt{2\left(a\,\frac{\mu_{eff}^2}{8}\,V(+4) + b\,\frac{\mu_{eff}^2}{8}\,V(+3)\right)}$$

where a and b are the proportions of vanadium(+4) and vanadium(+3) respectively, then 16% vanadium(+3) is necessary to explain the large effective moments. This is not consistent with TGA results. A comparison of percent vanadium(+3) determined by TGA and the method just described, Table 5-3, shows that the magnetic data consistently produces a higher percentage of reduced vanadium than do the TGA results. Therefore it appears that the enhancement of the effective moment above the spin-only value cannot be entirely accounted for by the presence of vanadium(+3) in these pyrochlores.

Table 5-3

A comparison of V(+3) content determined by TGA and the method outlined in text.

	From μ_{eff}		From TGA	
	V(+4)	V(+3)	V(+4)	V(+3)
$Y_{.4}Lu_{.6}$	.86	.14		
$Y_{.2}Lu_{.8}$	.83	.17		
$Sc_{.1}Lu_{.9}$	.84	.16		
$Sc_{.2}Lu_{.8}$	.83	.17		
$Sc_{.3}Lu_{.7}$	.70	.30	.99	.01
$Sc_{.4}Lu_{.6}$	.60	.40	.76	.24
$Sc_{.5}Lu_{.5}$	.50	.50	.66	.34

There have been other reports in the literature of 3d systems with higher than the expected spin-only moments. Reid and Sienko [1965] report an effective moment for $ScTiO_{3.003}$, a d^1 system, of 2.14 μ_B. This compound has a C - RE_2O_3 structure. The isostructural $ScVO_3$, a $3d^2$ system, also has an effective moment which is larger than the spin-only value. Casalot and Hagenmuller [1969] have investigated a series of compounds $Cu_xV_2O_5\beta$ ($.3 < x < .5$) and have shown that the copper incorporated into the V_2O_5 lattice loses an electron to V(+5) forming some V(+4). These compounds have effective moments of 1.91 μ_B to 1.98 μ_B, considerably larger than the spin only value. Still other materials with large effective moments are the d^5 perovskite species $CaRuO_3$, $SrRuO_3$ and $SrFeO_{3-x}$ [MacChesney et al., 1965; Goodenough, 1967]. While it appears there have been several compounds reported with effective moments higher than expected, there seems to be no quantitative theory with which to treat this problem.

The incorporation of vanadium(+3) into the lattice appears to alter the magnetic behavior at the end of the series $(Sc_xLu_{1-x})_2V_2O_7$, $x = .3, .4, .5$. The materials become more difficult to saturate and, for $x = .4$ and .5, do not saturate, even at 1.5 T, the highest field used. The effective moment can be seen to increase, as expected, with increasing vanadium(+3) content, while θ decreases. Since the Weiss constant is an indication of the algebraic sum of the exchange interactions, the incorpora-

tion of vanadium(+3) appears to add an antiferromagnetic term to the overall ferromagnetic sum. This is consistent with the properties of $ScVO_3$, which has the related C-RE_2O_3 structure and contains all vanadium(+3). Reid and Sienko [1965] reported susceptibility data in the range 80K < T < 300K. He found no evidence for ordering but the Weiss constant, -117K, indicates the predominance of antiferromagnetic interactions. Therefore it appears that the solid solutions, $(Sc_xLu_{1-x})_2V_2O_7$, $x = .3, .4, .5$, alter their behavior in a manner consistent with the incorporation of vanadium(+3). Since no critical temperature is available for $ScVO_3$ it is not clear what is causing the drop in T_c but it should be pointed out that this behavior is consistent with a disordering of the cations among the available sites in the pyrochlore structure as previously proposed [Greedan, 1979].

This investigation has determined that the behavior of the vanadium(+4) sublattice remains essentially constant over the cell dimensions studied. The small changes in the V-O bond lengths and V-O-V bond angles were not significant enough to noticeably affect the superexchange pathway.

There are few other oxides which have been reported to be simultaneously ferromagnetic and semiconducting. Recent studies on a series of perovskites $RETiO_3$; RE = La-Yb, Y have shown that $YTiO_3$ falls into this category [Garrett et al. 1981]. There are several similarities between the titanium perovskites and the vanadium pyrochlores. For example both vanadium(+4)

and titanium(+3) are $3d^1$ systems. Also the perovskite structure may be viewed as a network of distorted, corner sharing Ti-O octahedra similar to the V-O network found in $(RE)_2V_2O_7$.

Structural studies show the Ti-O-Ti bond angle decreases with the size of RE and at $YTiO_3$ is 142° [MacLean et al., 1979]. $LuTiO_3$, with a slightly smaller RE, has also been reported to be a ferromagnetic semiconductor [Bazuev et al. 1978b]. While no detailed structural data are available on $LuTiO_3$, the Ti-O-Ti bond angle, extrapolated from earlier members of the series, should be about 133.5°. This is close to the bond angles obtained for the pyrochlores.

The perovskite, unlike the pyrochlore structure, allows significant RE-Ti exchange interactions and the interpretation of the magnetic properties is more involved [Turner et al. 1981]. However, extensive work on the $RETiO_3$ system indicates a change in sign of the Ti-Ti exchange with the size of RE and therefore, the Ti-O-Ti bond angle. $LaTiO_3$ is an antiferromagnet [Goral, unpublished]. As RE varies through the series, the first unambiguous evidence for ferromagnetic Ti-Ti coupling occurs at $GdTiO_3$ and persists through to $YbTiO_3$ and possibly $LuTiO_3$ [Greedan,unpublished]. This suggests that the threshold Ti-O-Ti angle for ferromagnetic exchange is about 145°.

Using arguments outlined by Martin [1968],it appears the superexchange pathway discussed here should result in negative exchange interactions for an M-O-M bond angle of 180°. Interactions for M-O-M bond angle of 90° are difficult to

predict since there are both ferromagnetic and antiferromagnetic exchange pathways available. Furthermore, there appears to be no experimental evidence for ordering through a 90° superexchange pathway, probably because the M-M distances become close enough that direct exchange may not be ruled out. Unfortunately, the intermediate bond angles found in the $RETiO_3$ and $(RE)_2V_2O_7$ series render difficult any detailed calculations of exchange interactions.

CHAPTER 6

MAGNETIC NEUTRON DIFFRACTION

Introduction

The neutron has zero charge but a magnetic moment. Since the interaction between the neutron's magnetic moment and atomic magnetic moments is of the same order of magnitude as that between thermal neutrons and atomic nuclei, it is possible to examine the magnetic properties of the rare-earth atoms using elastic neutron scattering. It was argued in Chapter 4 that the magnetization data could not distinguish between ferromagnetic, ferrimagnetic, or a more complex ordering in $Tm_2V_2O_7$ and $Yb_2V_2O_7$. This chapter deals with neutron diffraction determination of the type of ordering and the rare-earth moment in $Yb_2V_2O_7$. After a discussion of the data treatment, ferromagnetic and ferrimagnetic models are compared with the experimental magnetic intensities.

Magnetic reflections result from the interaction of the moment of the neutron with unpaired electrons. In the case of ordered magnetic materials it is possible to have coherent scattering from aligned moments as well as from the chemical lattice. When the neutron beam is unpolarized, and the moments are colinear, the intensities of the Bragg peaks are additive [Bacon, 1977]

$$|F_{hk\ell}|^2 = F_{nuc}^2 + q^2 F_{mag}^2 \qquad (6\text{-}1)$$

$$= |\sum_n \bar{b}_n \exp(i\phi)|^2 \exp(-2w) +$$

$$q^2 |\sum_n p_n \exp(i\phi)|^2 \exp(-2w)$$

where ϕ is the phase angle

$$\phi = 2\pi \left(\frac{hx_n}{a} + \frac{ky_n}{b} + \frac{\ell z_n}{c}\right) .$$

$\exp(-2w)$ is the Debye-Waller factor and is assumed independent of n. $\bar{b}_n$ is the average nuclear scattering length at the n^{th} site. p_n is the magnetic scattering length

$$p = \frac{e^2\gamma}{2mc^3} gJf \qquad (6\text{-}2)$$

where e is the charge and m is the mass of an electron, c is the speed of light and γ is the magnetic moment of the neutron; equal to 1.913 nuclear magnetons [Squires, 1978]. gJ represents the atomic moment and f is the form factor for the unpaired electrons, which depends on the angle of scattered neutrons, 2θ. q is the magnetic interaction vector and is defined such that [Bacon, 1975],

$$q^2 = \sin^2\alpha \qquad (6\text{-}3)$$

where α is the angle between the scattering and magnetization vectors. In the absence of an external field, the magnetiza-

tion vectors in the crystallites are oriented such that $\langle \sin^2\alpha \rangle = \frac{2}{3}$ in a cubic material.

Model magnetic structures may be proposed, F^2_{mag} calculated, and the models refined to obtain the best agreement with F^2_{mag} obtained from the experiment.

The type of ordering can often be determined by examination of the powder pattern at $T < T_c$. If the chemical and magnetic cells are the same size, all magnetic reflections can be indexed with integral hkℓ values. Also, if the magnetic reflections have systematic absences consistent with the chemical unit cell, no symmetry elements have been removed. This would be the case for either the ferromagnetic or ferrimagnetic models outlined in Chapter 4. A more complicated spin arrangement would result in a magnetic cell larger than the chemical cell and, therefore, extra peaks. Ferromagnetic and ferrimagnetic ordering can only be distinguished by examining the intensities of the magnetic reflections, and comparing them to calculated intensities.

By comparing Bragg diffraction patterns above and below T_c it is possible to determine the scattering which results from aligned atomic moments. The positions and intensities of the peaks yield information about the type of ordering and the magnitude of the moments which are involved in the scattering. This experiment was done in an effort to determine the type of ordering and, if possible, the magni-

tude of the rare-earth moment, in $Yb_2V_2O_7$.

Data Treatment

Powder patterns were obtained at 100K and 7K. The 7K pattern is shown in Fig. 6-1. All peaks were indexed on the Fd3m chemical cell. Comparison of the two patterns indicated that the intensities of only a few 7K reflections were measurably enhanced. Four of these reflections were chosen, based on their ability to differentiate the two models predicted in chapter 4, and their intensities redetermined with a much smaller statistical error.

The magnetic intensities were determined from

$$I_{hk\ell}(7K) - I_{hk\ell}(100K) = I_{hk\ell}(mag) \qquad (6\text{-}3)$$

with the assumption that the Debye Waller factor in Eq. (6-1) was constant over the range used. The scale factor was obtained from 100K data. Scattering lengths were taken from Bacon [1975] and magnetic form factors for vanadium and ytterbium from Freeman and Watson [1961] and Stassis et al. [1977] respectively. Agreement factors [Buerger,1960]

$$R = \frac{\Sigma(F_{obs}-F_{calc})^2}{\Sigma F_{obs}^2} \qquad (6\text{-}4)$$

were used to indicate how well the model fit the experimental data. The structure factor, F, was obtained by

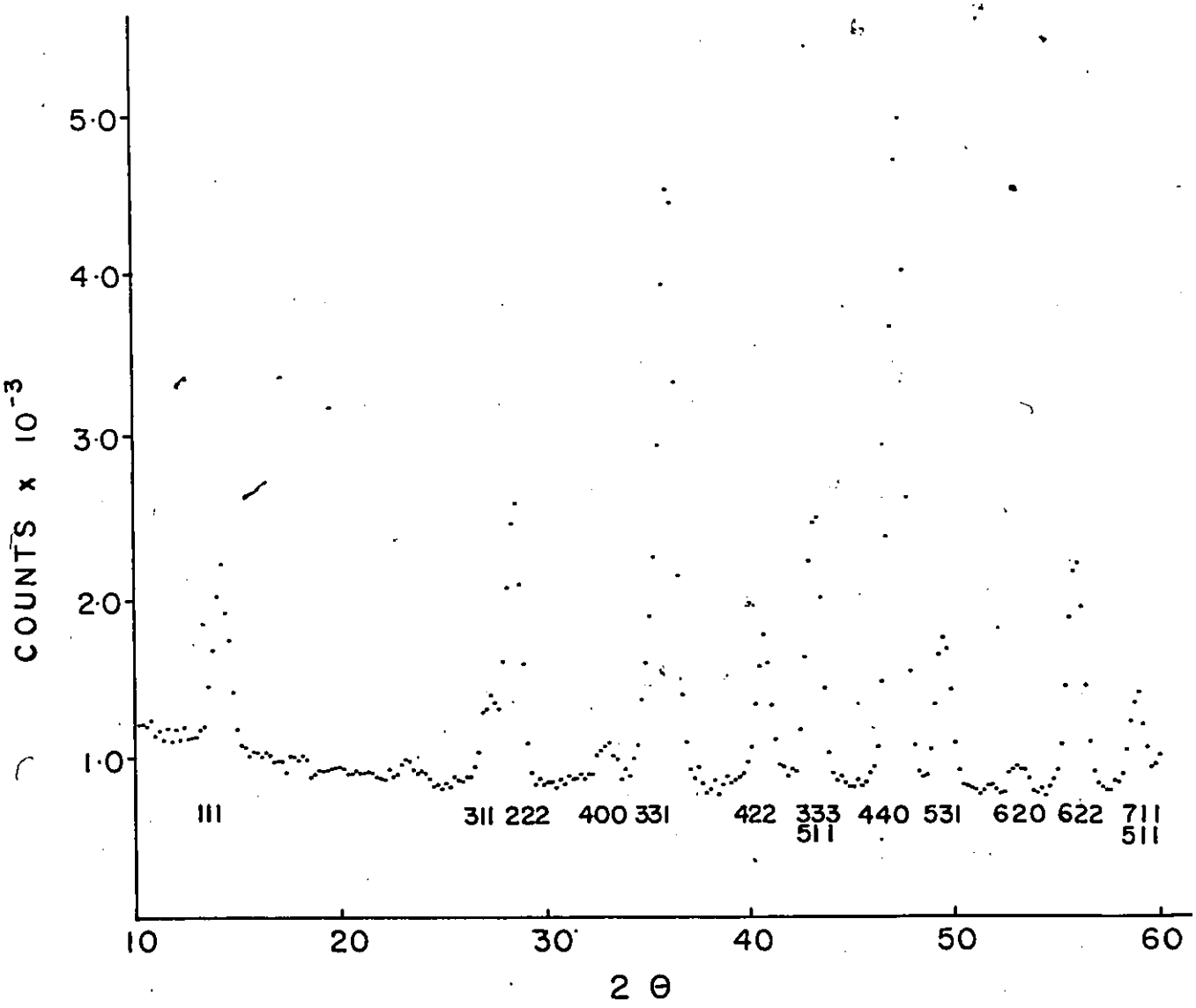

Figure 6-1 Neutron powder diffraction pattern for $Yb_2V_2O_7$ at 7K.

$$F_{obs} = \sqrt{\frac{I_{obs}}{jL}} \qquad (6\text{-}5)$$

where j is the multiplicity and L is the Lorentz correction

$$L = \frac{1}{\sin 2\theta} .$$

Absorption was omitted from Eq. (6-5) since this correction is small (see Chapter 3).

Discussion

Complex magnetic structures were eliminated when no extra peaks were observed in the 7K data. However there are still two models which are consistent with this observation. One is parallel alignment of all the spins, termed the ferromagnetic model, and the other is parallel alignment of the Yb(3+) spins which are antiparallel to the vanadium spins, called the ferrimagnetic model.

The vanadium moment, used in all calculated intensities, was taken to be 0.94 μ_B, as determined from saturation magnetization data for $Lu_2V_2O_7$ [Soderholm and Greedan, 1979a]. The ferrimagnetic model assumed a Yb(+3) moment of 3.4 μ_B, and the initial ferromagnetic model a moment of 1.7 μ_B consistent with the saturation magnetization data discussed in Chapter 4. The intensities for the two different coupling schemes were calculated using these moments, and the oxygen x parameter determined from the atomic structure (Chapter 3). The results are shown in Table 6-1.

Table 6-1

Calculated and experimental neutron intensities for $Yb_2V_2O_7$

hkℓ	I_{obs}(100K)	I_{obs}(7K)	I_{obs}(mag)	I^{ferro}_{calc}	I^{ferri}_{calc}
111	473(8)	471(8)	-2(11)	13	359
222	619(7)	716(7)	97(11)	102	120
400	89(7)	147(7)	58(9)	52	67
440	1729(8)	1767(8)	38(12)	36	78
		R* (agreement factor)		1.6%	40%

*see Equation (6-4) in text.

Although the uncertainties in I_{obs}(mag) are large, the data are in clear agreement with the ferromagnetic model and are not compatible with the ferrimagnetic model. Ferrimagnetic coupling predicts that I_{111}(mag) will be the strongest magnetic reflection, whereas ferromagnetic coupling predicts the same reflection to be weak. In fact the peak must be classed as unobserved. However, the ferromagnetic model only predicts a peak one standard error above background. Agreement factors are also listed and indicate the clear superiority of the ferromagnetic model. The magnitude of the Yb(+3) moment was varied and, from fitting to three observed reflections, determined to be $1.7\pm.2\ \mu_B$. This is in good agreement with the saturation magnetization data for $Yb_2V_2O_7$.

These data are consistent with that expected for ferromagnetic coupling of all moments. Unfortunately no information is available on the crystallographic direction of the moments because, for powder data, a moment direction can only be determined with respect to a unique crystallographic axis [Shirane, 1959]. Since $Yb_2V_2O_7$ is cubic, there is no unique crystal axis.

No attempt was made to determine the moment ordering in the case of $Tm_2V_2O_7$ because the moment is expected to be even smaller than that obtained for $Yb_2V_2O_7$. Since all magnetic reflections are superimposed on nuclear peaks, it was felt that it would be difficult to obtain statistically meaningful data. However, there is no reason to assume that

$Tm_2V_2O_7$ does not order ferromagnetically.

It now appears that the moment on Yb(+3) is 1.7 μ_B. The low saturation moments for $Yb_2V_2O_7$ and $Tm_2V_2O_7$ may be the result of interactions with the crystalline electric field. This possibility is dealt with in the next chapter.

CHAPTER 7

THE EFFECT OF THE CRYSTALLINE ELECTRIC FIELD

Introduction

Magnetic neutron diffraction data have been interpreted as consistent with ferromagnetic ordering in $Yb_2V_2O_7$ [Soderholm et al. 1980]. The magnetic moment of Yb(+3) was determined to be $1.7\pm.2\ \mu_B$, in good agreement with the saturation magnetization, but much lower than the $4.0\ \mu_B$ expected for a free ion. It has been postulated that this low moment might result from interaction with the crystalline electric field. Calculations on the effect of the interaction between the crystalline electric field and the rare earth magnetic moments are discussed in this chapter. An attempt is made to explain the low saturation moments as well as the shape of the M vs T and χ^{-1} vs T curves for $Yb_2V_2O_7$ and $Tm_2V_2O_7$ in terms of this interaction.

The electrostatic potential at a point (r,θ,ϕ) near the origin at the nucleus of the rare-earth ion, resulting from surrounding point charges, may be expressed as [Boudreaux and Mulay, 1976]

$$V(r,\theta,\phi) = \sum_i q_i/(\underline{R}_i-\underline{r}) \qquad (7\text{-}1)$$

where q_i is the charge on the i^{th} neighbour at a distance R_i.

If the rare-earth has a charge q_k at (r',θ',ϕ'), the electrostatic energy, resulting from the perturbation potential, is

$$H_{CEF} = \sum_k q_k V = \sum_k \sum_i q_k q_i / (\underline{R}_i - \underline{r}_k) \ . \qquad (7\text{-}2)$$

For the case of rare earth ions, except Eu and Sm, the splitting of the free ion term, caused by spin orbit coupling, is considered a larger perturbation than the crystal field so the Hamiltonian may be written:

$$H_{RE} = H_{\text{Free ion}} + H_{CEF} - \bar{\mu}\cdot\bar{H} \ , \qquad (7\text{-}3)$$

where $H_{\text{Free ion}}$ includes spin-orbit coupling. This permits calculation over only the ground state multiplet. Stevens [1952] made use of the large splitting between multiplets in his method of operator equivalents. This method involves replacing x,y,z by $\bar{J}_x$, $\bar{J}_y$, $\bar{J}_z$, while being careful to account for non-commutation of these operators. Using this method the crystal field Hamiltonian may be rewritten [Hutchings, 1964]

$$H_{CEF} = \sum_{n=0}^{n'} \sum_{m=-n}^{n} B_n^m O_n^m \qquad (7\text{-}4)$$

where $n' = 6$ for rare earth ions. Here O_n^m's are the Stevens operator equivalents. They represent polynomials of the angular momentum operators and are tabulated for different J values by Hutchings. The B_n^m's, sometimes refetred to as crystal field intensity parameters, are determined by the surrounding ions as well as the radial extension of the 4f electrons, $\langle r^n \rangle$ and the

total angular momentum, $\langle J||\theta_n||J\rangle$, of the rare-earth ion:

$$B_n^m = A_n^m \langle r^n \rangle \langle J||\theta_n||J\rangle \quad . \qquad (7\text{-}5)$$

Here A_n^m represents the lattice sum and $\langle J||\theta_n||J\rangle$ are reduced matrix elements, usually designated α, β, γ for $n = 2,4,6$ and tabulated in Hutchings [1964]. The total number of independent, non-zero crystal field parameters may be limited by the site symmetry.

Two groups investigated the pyrochlore $Yb_2Ti_2O_7$. In this case the only magnetic ion is Yb(+3). The site symmetry of the rare-earth is $\bar{3}m$ which leads to a crystal field Hamiltonian:

$$H_{CF} = B_2^0 O_2^0 + B_4^0 O_4^0 + B_6^0 O_6^0 + B_4^3 O_4^3 + B_6^3 O_4^3 + B_6^6 O_6^6 \quad . \qquad (7\text{-}6)$$

Dunlap et al. [1978] truncated this Hamiltonian to the following axial version:

$$H_{CF} = B_2^0 O_2^0 + B_4^0 O_4^0 \qquad (7\text{-}7)$$

to explain the magnetic field dependence of ^{170}Yb Mössbauer spectra. They found a $|\pm 3/2\rangle$ ground state with the first excited state, $|\pm 1/2\rangle$, at 18K. Townsend et al. [1968] interpreted susceptibility data on the same compound in the range 2 - 1400K using a cubic crystal field Hamiltonian with an added axial term

$$H_{CF} = B_2^0 O_2^0 - \frac{2}{3} B_4^0 (O_4^0 - 20\sqrt{2}\, O_4^3) + \frac{16}{9} B_6^0 (O_6^0 + \frac{32\sqrt{2}}{4} O_6^3 + \frac{77}{8} O_6^6) \quad . \qquad (7\text{-}8)$$

They found, for the cubic Hamiltonian, a Γ_7 ground state with a first excited state, Γ_6, at 1040K. Townsend et al. varied the B_2^0 term from zero until it was as large as the B_4^0 term and found the fit to experimental data was insensitive to the second order term.

Clearly these two energy level schemes are not consistent. Since the Yb(+3) ion is in the same environment in both the titanium and vanadium pyrochlores it was felt that the crystal field calculations on $Yb_2V_2O_7$ and $Tm_2V_2O_7$ might prove helpful in resolving this discrepancy as well as explaining the magnetic properties of the vanadium pyrochlores.

Calculated Susceptibilities

To examine the contribution of the rare-earth sublattice to the magnetic properties in $Yb_2V_2O_7$ and $Tm_2V_2O_7$, it is necessary to account for the behaviour of the vanadium sublattice. Since the critical temperature appears to be independent of the rare earth, the vanadium-vanadium interaction is assumed to be constant over the three pyrochlores. It can therefore be determined directly from $Lu_2V_2O_7$ where Lu(+3) is a $^1S_0$ ion. Molecular field theory treats the problem of two interpenetrating sublattices by assuming that an average internal field is generated which may be represented by:

$$H_M^V = \lambda_{VV} M_V + \lambda_{RV} M_R$$
$$H_M^R = \lambda_{RV} M_V + \lambda_{RR} M_R \qquad (7\text{-}9)$$

λ_{VV} and λ_{RR} represent the intrasublattice coupling in the vanadium and rare earth sublattices and λ_{RV} the intersublattice coupling. M_V and M_R are the magnetizations of the two sublattices. Since the critical temperatures of the vanadium pyrochlores are almost independent of the rare earth and $Yb_2Ti_2O_7$ (Ti(+4) is d^0) does not order down to 4K [Dunlap et al. 1978], λ_{RR} was assumed to be negligible and λ_{RV} small compared to λ_{VV}. The molecular fields were then simplified

$$H_M^R = \lambda_{RV} M_V$$
$$H_M^V = \lambda_{VV} M_V \quad . \tag{7-10}$$

All the data for $Yb_2V_2O_7$ and the $T > T_c$ data for $Tm_2V_2O_7$ were treated using the assumption that the vanadium contribution could be subtracted directly, leaving only the molecular field $\lambda_{RV}M_V$ as an adjustable parameter. The paramagnetic susceptibility per rare-earth ion was therefore calculated using

$$2\chi_{exp}^{RE}(T) = \frac{M_{total} - M_{Lu_2V_2O_7}}{H_{ext} + \lambda_{RV}M_V} \quad . \tag{7-11}$$

Low temperature $Yb_2V_2O_7$ data, treated in this manner, are shown in Fig. 7-1.

A different procedure was used to determine χ_{exp}^{RE} at $T < T_c$ from the $Tm_2C_2O_7$ data. Since Tm(+3) has a small contribution to the total magnetization at these temperatures, the $M(Tm_2V_2O_7) - M(Lu_2V_2O_7)$ values were small, and experimental errors dominated.

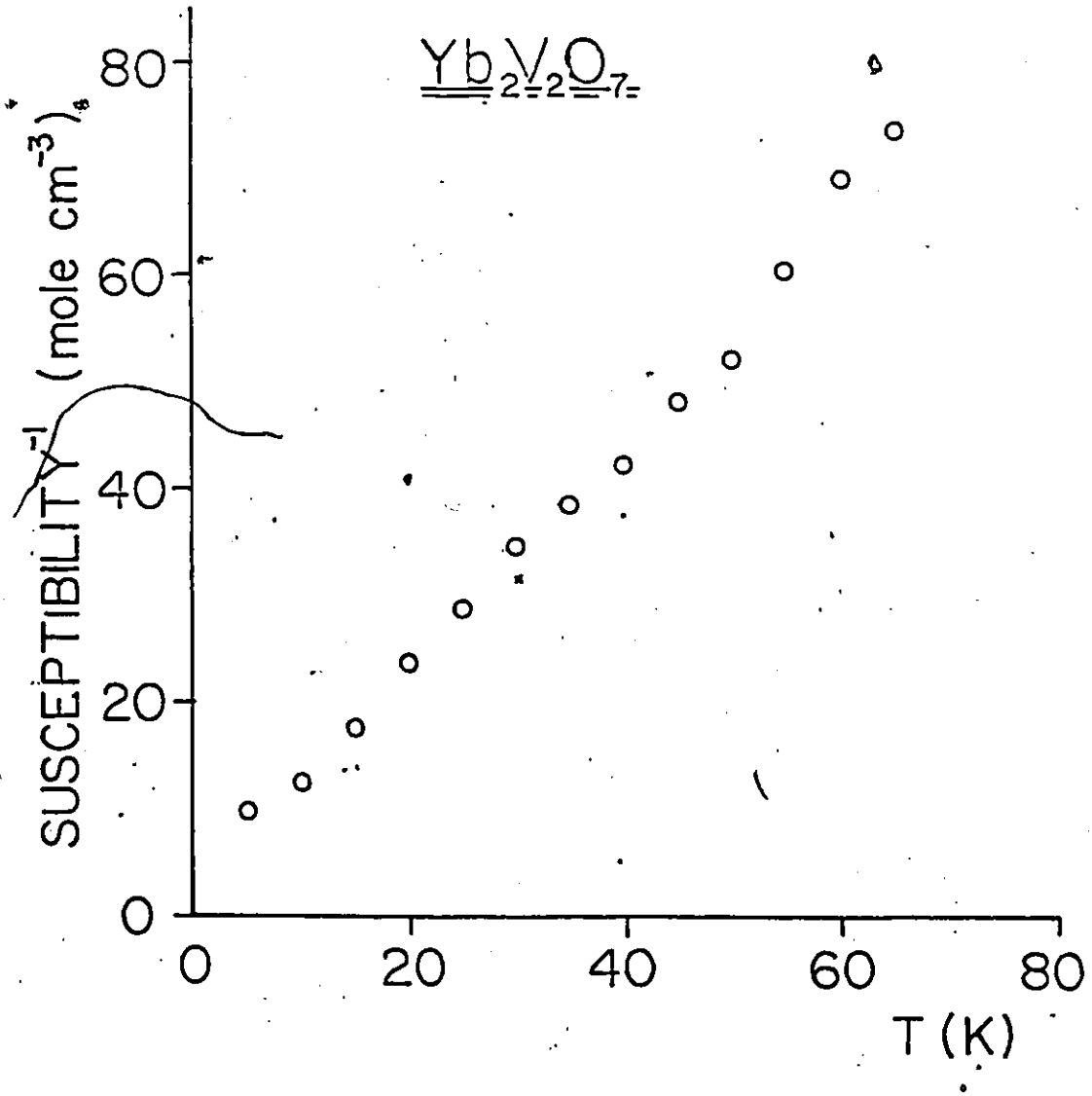

Figure 7-1 Low temperature inverse susceptibility versus temperature for $Yb_2V_2O_7$. The data have been corrected for RE-V exchange as outlined in the text.

Furthermore, it was difficult to estimate $M(Tm_2V_2O_7)$ because the M versus H curves did not saturate, even at 4K. Close examination of these curves, some of which are shown in Fig. 7-2, show a rectilinear high field region with a non-zero slope. The slope, $(\frac{\partial M}{\partial H})_T$, was interpreted as χ_{Tm} directly since the $Lu_2V_2O_7$ data indicated χ_V was almost zero at low temperatures. However, near T_c, the M versus H curves for $Lu_2V_2O_7$ do not saturate either and it was necessary to subtract a contribution to the susceptibility by the vanadium sublattice. This interpretation of the data also provides an independent estimation of λ_{RV} because $\chi^{Tm}_{exp} = \frac{M_{Tm}}{\lambda_{RV} M_V}$. For the low temperature $Tm_2V_2O_7$ susceptibilities it was necessary to estimate and subtract a diamagnetic contribution to χ^{Tm}_{exp}. When Eq. (7-11) was used the diagmagnetic contribution was removed by the subtraction of $M(Lu_2V_2O_7)$.

The experimental susceptibility data were interpreted by fitting to a theoretical model using the van Vleck formalism [van Vleck, 1932]

$$\chi^{RE}_{theo} = \frac{N_0}{kTZ} \sum_i \left[|\langle \psi_i | \bar{\mu} | \psi_i \rangle|^2 - 2 \sum_{j \neq i} \frac{|\langle \psi_i | \bar{\mu} | \psi_j \rangle|^2}{E_i - E_j} kT \right] e^{-E_i/kT} \qquad (7\text{-}12)$$

$$Z = \sum_i e^{-E_i/kT}$$

discussed in Chapter 1, where g_J is the free ion gyromagnetic ratio. The first order matrix element represents the Zeeman splitting while the second order term is the temperature independent van Vleck susceptibility arising from states mixing in

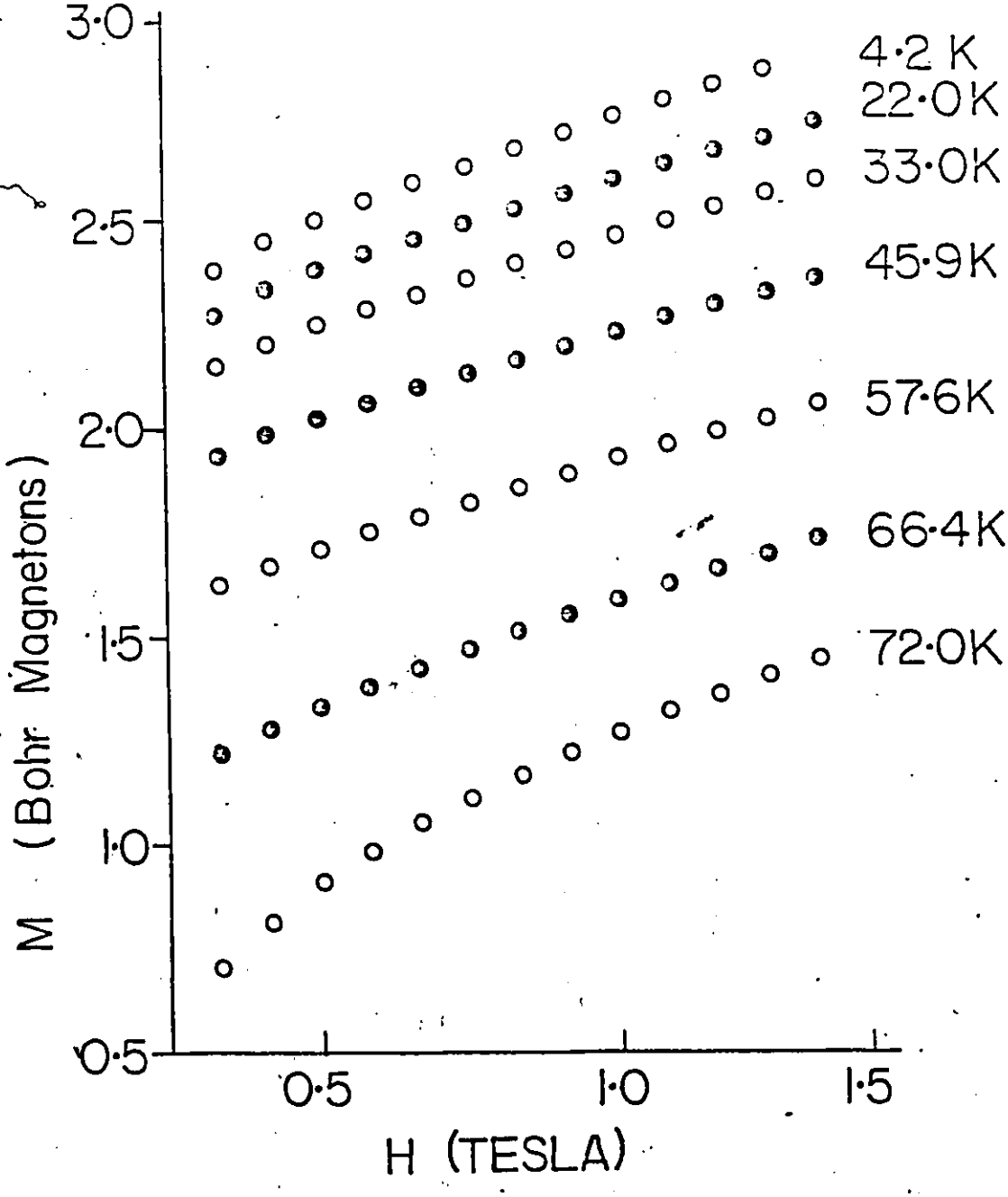

Figure 7-2 Magnetic moment, per $Tm_2V_2O_7$, versus field curves taken at various temperatures. The slopes of these curves were used to determine the Tm(+3) susceptibility.

a magnetic field. The E_i's represent the splitting resulting from the crystalline electric field.

The eigenfunctions and eigenvalues were obtained using perturbation theory as outlined previously. Since the site symmetry of the rare-earth is $\bar{3}m$ the crystal field Hamiltonian is

$$H_{CEF} = B_2^0O_2^0+B_4^0O_4^0+B_4^3O_4^3+B_6^0O_6^0+B_6^3O_6^3+ B_6^6O_6^6 \quad (7\text{-}13)$$

Cubic site symmetry was assumed in order to limit the number of adjustable parameters, so the Hamiltonian used was

$$H_{CEF} = B_4^0[O_4^0-20\sqrt{2}O_4^3] + B_6^0[O_6^0 + \frac{35\sqrt{2}}{4} O_6^3 + \frac{77}{8} O_6^6] \quad (7\text{-}14)$$

where the trigonal axis is chosen as the Z-axis. Initial values of B_n^m's were obtained from nearest neighbour point charge calculations. The Hamiltonian was diagonalized to obtain eigenvectors and energy spacings, the susceptibility calculated and this procedure iterated to obtain the best fit. Comparisons of experimental and calculated susceptibilities are shown in Figs. 7-3, 7-4.

The possible energy level separations in the case of cubic symmetry, can be characterized by two parameters, an energy scaling and a ratio of the fourth to sixth order crystal field terms. Lea, Leask and Wolf [1962] related these to two parameters W and X, which they plotted for different f-electron terms. These plots proved very useful as a check of the computer diagonalization procedure. The results are shown in Table 7-1.

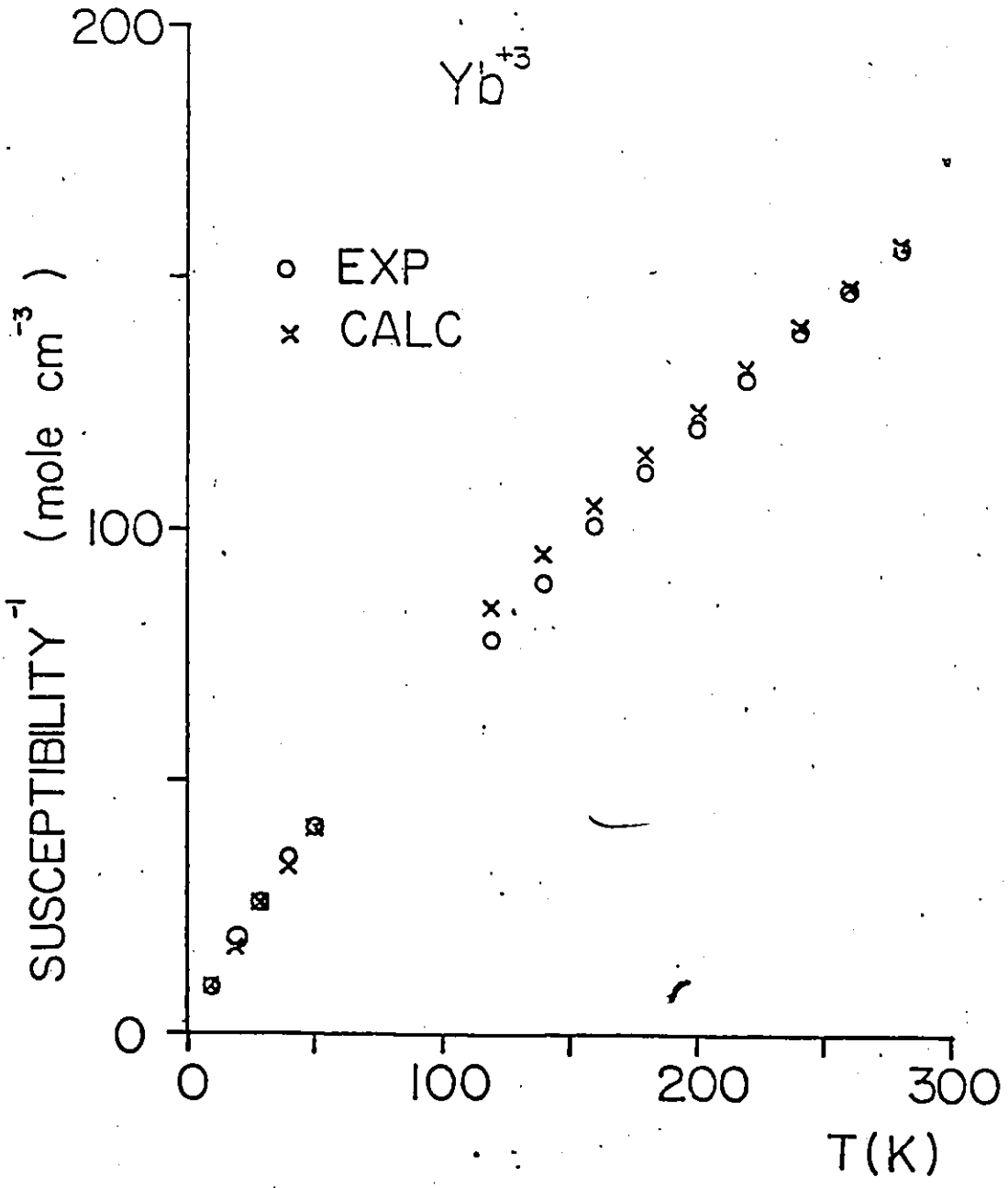

Figure 7-3 A compression of the calculated and experimental inverse susceptibilities for Yb(+3). The critical temperature is 73.2K.

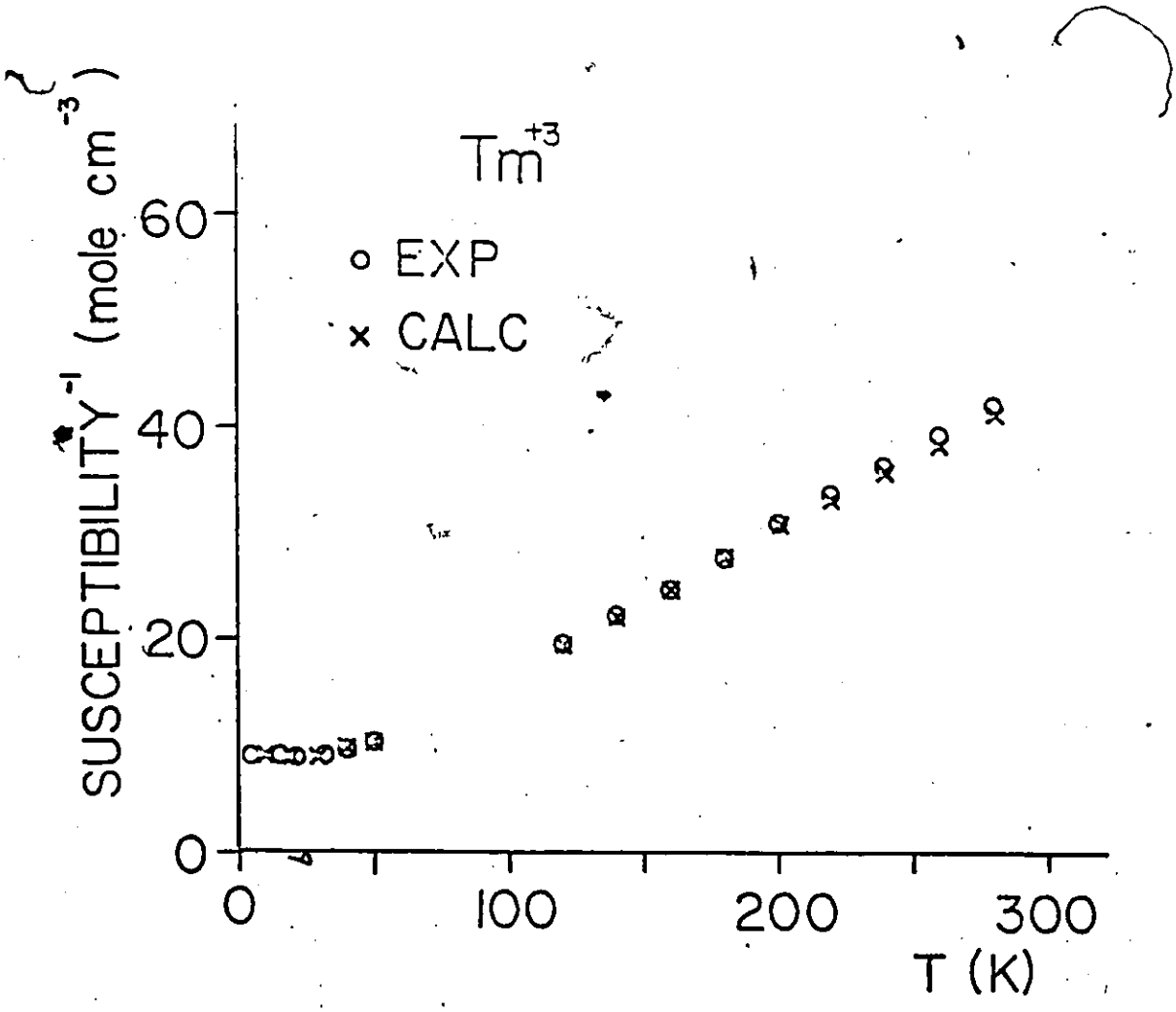

Figure 7-4 A comparison of the calculated and experimental inverse susceptibilities for Tm(+3). The critical temperature is 71.4K.

Table 7-1

Crystal Field Parameters for Tm(+3) and Yb(+3)

	Tm(+3)	Yb(+3)	Yb(+3) in $Yb_2Ti_2O_3$ [Townsend et al. 1968]
W	-4.114	60	-
X	0.65	.95	-
λ^*_{RV}(mole cm^{-3})	2.5	14	-
B_4^{0+}(K)	0.0297	-0.633	-0.498
B_6^0(K)	-0.000339	0.000705	0.00719
A_4^0(K)	170	380	300
A_6^0(K)	16.6	1.53	1.56

+ these values are based on the threefold axis as the z-axis. The conversions to the B's used by Lea, Leask and Wolf are:

$$B_4^{0(LLW)} = -3/2\ B_4^0$$

$$B_6^{0(LLW)} = 9/16\ B_6^0$$

* λ in units of moles of vanadium ions per cm^3.

Discussion

Yb(+3), a Kramers ion with a $^2F_{7/2}$ ground term, is expected to split into two doublets and a quartet in a cubic crystal field. The best fit to the data places the Γ_7 doublet as the ground state with the quartet Γ_8 1100K above the ground state and $E_{\Gamma_6} - E_{\Gamma_7}$ at approximately 1800K.

Attempts were also made to fit the Yb(+3) data to the axial Hamiltonian, Eq. (7-7), chosen by Dunlap et al. [1978]. The magnetization versus temperature data, below T_c, fit well to an axial model with $|\pm 3/2\rangle$ as the ground state and $E_{|1/2\rangle} - E_{|3/2\rangle} = 37K$. This is in reasonable agreement with Dunlap's splitting of 18K. However, this axial model could not be reconciled with higher temperature data, where it predicted free ion behaviour.

The axial and cubic models both predict a ground state moment of 1.7 μ_B, in agreement with the 4K saturation magnetization as well as the interpretation of neutron diffraction [Soderholm et al., 1980] and Mössbauer data.

Tm(+3), with an $^3H_6$ ground term, has an even number of electrons and, in a cubic crystal field, is split into three triplets, a doublet and two singlets. The energy level ordering obtained from the fitting procedure is shown in Fig. 7-5. The temperature independence of the low temperature data is accounted for by a ground state singlet, Γ_2, with a triplet, Γ_5, 140K above the ground state.

Values of the coupling constants λ_{RV}, in terms of moles of vanadium ions, were determined to be 14 mole cm^{-3} for YbV(+3)

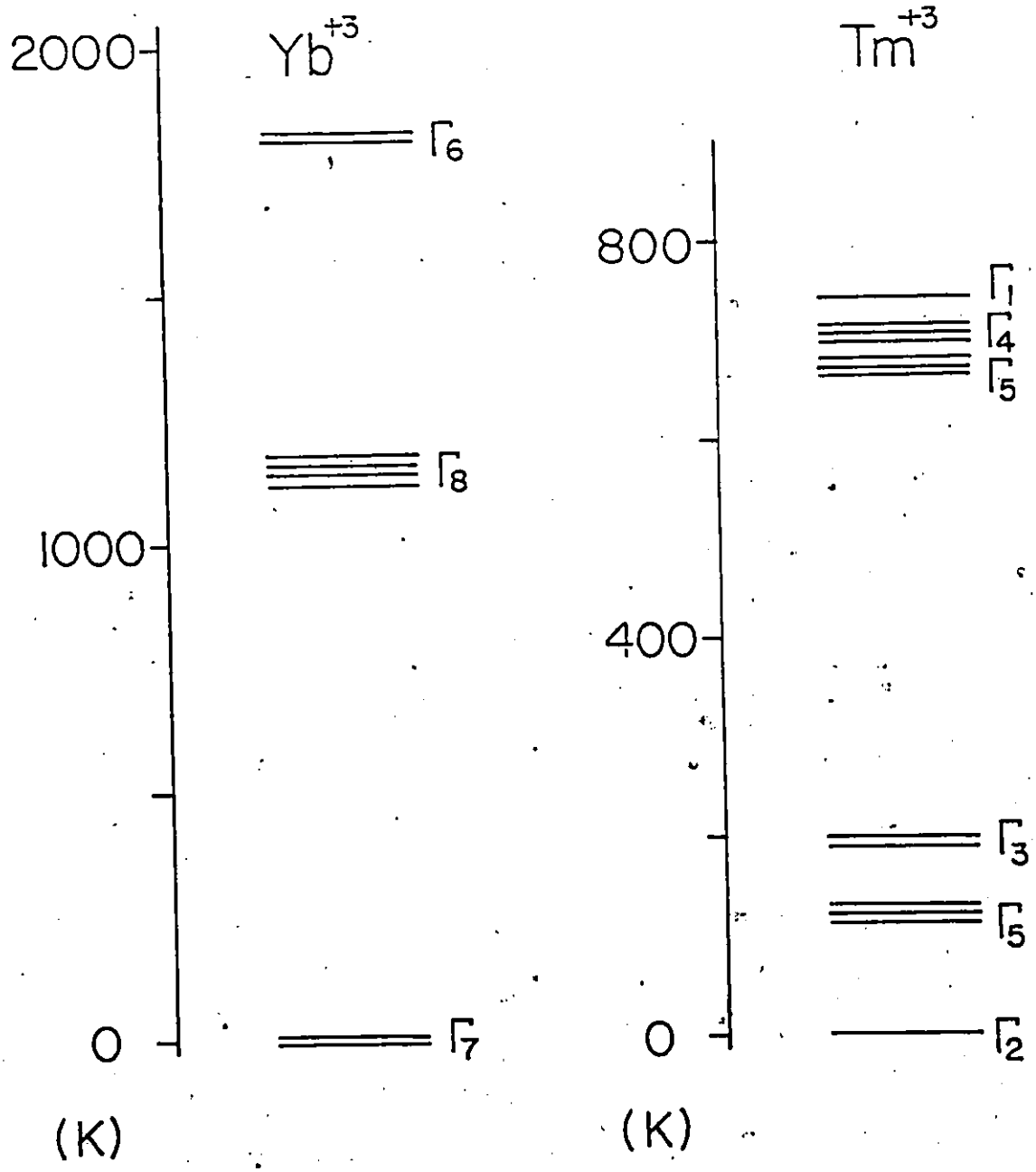

Figure 7-5 Calculated energy level diagrams for Yb(+3) and Tm(+3).

and 2.5 mole cm^{-3} for Tm(+3). These values can be compared to 580 mole cm^{-3} obtained for λ_{VV} from the mean field expression for the critical temperature

$$T_c = \frac{\mu \lambda_{VV} M_V}{3K} \quad . \qquad (7\text{-}15)$$

These results support the argument that the interaction of vanadium atoms is the driving force for the magnetic ordering.

A_n^m's depend only on the rare-earth environment and should be independent of the lanthanide ion. Dunlap and Shenoy [1975] fit susceptibilities in a series of cryolites Cs_2NaRCl_6, where R is a rare-earth ion in cubic site symmetry, and found the A_n^m's were indeed invariant to R, to within the experimental error. A comparison of A_n^m's for Tm(+3) and Yb(+3) in the vanadium pyrochlores shows a discrepancy in the A_4^0 terms with the most probable cause being the deviation of the site from cubic symmetry. The excited state triplet at 140K above the ground state, for the case of Tm(+3) in cubic symmetry, will be split into a doublet and a singlet in lower symmetry. As well as the addition of a B_2^0 term to the crystal field Hamiltonian, calculation of the splitting in non-cubic symmetry also relaxes the fourth and sixth order relationships. It was felt that the limited data did not justify the inclusion of four extra terms in the Hamiltonian.

The Yb(+3) quartet at 1100K is split into two doublets in $\bar{3}m$ symmetry, but this does not alter the calculated suscep-

tibility, even at 300K, because of the large energy denominator in the second-order term of Eq. (7-12). Rediagonalization of the crystal field Hamiltonian with an added B_2^0 term of 14K alters the ground state moment by less than 2%. Townsend and Crossley [1968], working with susceptibility data from $Yb_2Ti_2O_7$, found a similar behaviour in their calculations.

Hutchings and Wolf [1964] attempted to calculate energy level splittings of the J = 7/2 and J = 5/2 multiplets of Yb(+3) in yttrium gallium garnet using a point charge model. They had susceptibility, EPR, and some optical data to help in their analysis. The site symmetry of Yb(+3) is 222, therefore there were nine independent crystal field parameters. They found that a cubic approximation of the crystalline electric field fit the data well, with the insensitivity of the calculated values to deviations from cubic symmetry explained by the large energy splitting of the lowest lying Kramers doublet from all other states. The terms involving admixture of non-cubic parameters, they argue, are small and, to a first approximation, leave the ground state moment unchanged from the cubic value. They also state that for ions other than Yb(+3) the near cubic approximation has met with less success although there is still quantitative agreement with some of the striking features. These conclusions are supported by later work on this system by Pearson et al. [1967].

The calculations discussed in this chapter have assumed that the Yb(+3) and Tm(+3) moments are paramagnetic over the temperature range studied. The vanadium atoms, which order at

about 70K, generate an internal field that acts on the rare-earth moments, resulting in the net magnetization observed by neutron diffraction.

Similar behaviour has been reported for a series of distorted perovskites, $RCrO_3$ (R = Pr, Sm, Tb, Dy and Ho) [Hornreich, 1978]. The coupling of magnetic moments between Cr(+3) nearest neighbours, through a super exchange pathway, as outlined in Chapter 5, is predominantly antiferromagnetic, although below T_c they all exhibit a weak ferromagnetic moment. Except for the spin reorientation regions, the ferromagnetic moment lies along the crystallographic a direction. The rare-earth moments, if they exhibit any collective order at all, order at temperatures much below the critical temperature of the chromium sublattice. $HoCrO_3$, for example, shows no cooperative ordering of the Ho(+3) spins down to at least 1.5K [Hornreich et al. 1972], although the chromium moments order at 140K. The small Ho-Cr coupling constant is substantiated by the similarity of ordering temperatures between $HoCrO_3$ and $YCrO_3$, which orders at 141K [Judin and Sherman, 1966].

Although the $RCrO_3$ series have paramagnetic R atoms, it should be pointed out that the isostructural titanium series, $RTiO_3$ (R = rare earth), have comparable R-Ti and Ti-Ti exchange interactions [Turner, 1982]. The moments on both sublattices order at the same temperature, although it should be noted that the critical temperatures are much lower in the titanium than in the chromium series.

Although it is believed that there is no cooperative long range ordering of the rare earth sublattices in either the chromium perovskites or the vanadium pyrochlores, and that the rare-earth-transition metal coupling is small, there is some evidence for weak R-M exchange interactions. In the case of both $Yb_2V_2O_7$ and $Tm_2V_2O_7$ the RE-V exchange is positive and the moments lie parallel while the magnetic ordering in the chromium perovskites is actually relatively complex. In conjunction with the canted spin arrangement of the chromium spins, the coupling in the RE sublattice also involves both antiferromagnetic components. The ferromagnetic component is in the a direction. These small ferromagnetic components on the two magnetic sublattices are aligned parallel.

Positive exchange interactions between rare-earth and transition metals are unusual. Several detailed investigations have been carried out on rare-earth-ion exchange interactions in a series of garnets $R_3Fe_5O_{12}$ (R = Sm-Lu,Y). These compounds crystallized in the cubic space group Ia3d with 8 formula units per unit cell [Geller and Gilleo, 1959]. The iron atoms sit on two different crystallographic sites, one octahedrally and the other tetrahedrally coordinated. The 4K saturation moment of the iron sublattice was determined [Bertaut and Forrat, 1956; Geller and Gilleo, 1957] to be slightly less than 5 μ_B per formula unit. The spin only moment for Fe(+3) is 5 μ_B. It is believed [Gilleo, 1980] that this moment results from the antiferromagnetic superexchange between the three Fe(+3) atoms

on the tetrahedral sites and the two Fe(+3) on the octahedral sites. Gilleo [1980] argues that the exchange field produced by this net iron moment acts only on the spin component of the unpaired rare-earth electrons. According to Hund's Third Rule, the total moment on the rare earth is $J = L-S$ when the outer electron shell is less than half filled, and $J = L+S$ if it is more than half filled. It is assumed that the spins on the rare-earth and the iron atoms couple antiparallel [Taylor and Darby, 1972]. If $L > 2S$, as is the case for Ho → Yb, then the total rare earth moment should couple antiparallel to the net iron spin, as shown in Fig. 7-6, and the magnetization versus temperature curve should have a compensation temperature. This has indeed been found to be the case [Bertant and Pauthenet, 1957]. Unfortunately the lighter lanthanides do not form iron garnets but several solid solutions of lighter rare-earths with non magnetic ions, such as Y(+3) and Lu(+3), have been investigated. Geller et al. [1961] studied $Nd_{1.5}Y_{1.5}Fe_5O_{12}$ and found parallel coupling of the total Nd(+3) moment and the Fe(+3) spin. This is in agreement with the proposed mechanism for coupling in these materials.

According to the mechanism outlined for the rare-earth-iron coupling in the garnets, both the ytterbium and thulium pyrochlores should have antiparallel coupling of the moments on the two sublattices, which is not the case. Even the spin components of the two magnetic species lie parallel. Although

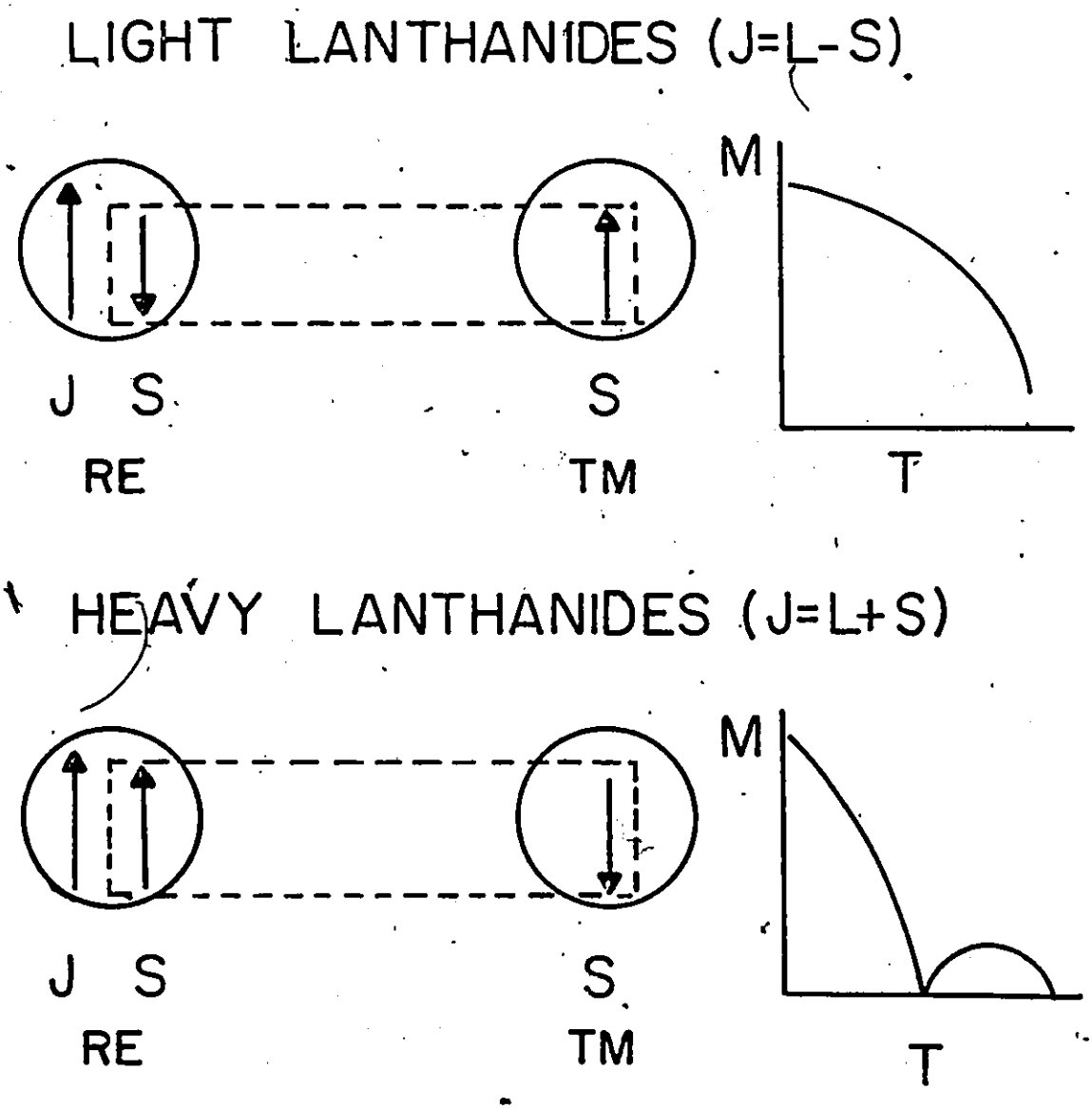

Figure 7-6 The rare-earth-transition metal coupling scheme proposed for the garnets [Gilleo, 1980].

no vanadium pyrochlores have been synthesized with rare-earths larger than thulium, it would be interesting if one could obtain a solid solution of a light rare-earth with lutetium, for example $(Nd_xLu_{1-x})_2V_2O_7$, to see if there was a change in sign of the RE-V exchange interaction.

CHAPTER 8

^{170}Yb MÖSSBAUER ON $Yb_2V_2O_7$

Introduction

Calculations discussed in the previous chapter have shown that the magnetic behaviour of the Tm(+3) and Yb(+3) atoms in the pyrochlore structure is consistent with that expected of a rare-earth ion in a cubic crystal field. The calculated values appear insensitive to the addition of a B_2^0 term, although cubic restrictions on the ratios $B_4^0:B_6^0$ and $B_6^0:B_6^3:B_6^6$ were not relaxed [Soderholm et al., 1982]. This is a surprise since the crystal structure indicates that the rare-earth site has highly axial symmetry. Although magnetic data may be insensitive to the B_2^0 term, it can be determined independently by Mössbauer spectroscopy since the magnitude of the electric field gradient (EFG) is directly proportional to B_2^0.

In addition to evaluating B_2^0, Mössbauer spectroscopy can also be used to determine the moment on Yb(+3) directly. All the other techniques discussed previously required that a moment be assumed for the vanadium atoms. Therefore ^{170}Yb Mössbauer spectra were obtained for $Yb_2V_2O_7$ both to confirm the magnetic moment of Yb(+3) and to determine a value for B_2^0.

Pertinent information on ^{170}Yb is shown in Table 8-1. The nuclear ground state is non-degenerate; however the excited state, with I = 2, has both a quadrupole and magnetic moment. The magnetic moment will interact with a surrounding effective field and the quadrupole moment will interact with any asymmetry in the extranuclear charge distribution.

The interaction Hamiltonian will have the form

$$\hat{H} = \hat{H}_{\text{free ion}} + \hat{H}_{cf} + \hat{H}_z + \hat{H}_{hf} \qquad (8\text{-}1)$$

where $\hat{H}_{\text{free ion}}$ and $\hat{H}_{cf}$ are described elsewhere (see Eqs. 7-3, 7-6), $\hat{H}_z$ is the Zeeman term and

$$\hat{H}_{cf} > \hat{H}_z > \hat{H}_{hf} .$$

$\hat{H}_{hf}$ represents the hyperfine Hamiltonian and may be expressed as

$$\hat{H}_{hf} = \hat{H}_Q + \hat{H}_M . \qquad (8\text{-}2)$$

Here $\hat{H}_Q$ and $\hat{H}_M$ represent the quadrupolar and magnetic hyperfine interactions respectively.

The electric field gradient (EFG) at the nucleus may be expressed as a (3×3) second-rank traceless tensor. The axes are chosen such that all off-diagonal elements are zero, and the ordering of the principal axes are

$$|V_{zz}| \geq |V_{xx}| \geq |V_{yy}| . \qquad (8\text{-}3)$$

Table 8-1

Nuclear data for ^{170}Yb*

Energy of transition	E_γ (keV)	84.26
Natural line width	$2\Gamma_{nat}$ (mm sec^{-1})	2.01
Nuclear spin quantum numbers		
ground state	I_g	0
excited state	I_e	2
Magnetic moment		
excited state	μ_e (μ_N)	+0.67
Quadrupole moment of		
nucleus	Q_e (barns)	-2.14
Natural abundance		
^{170}Yb		3.0

*reference [Lederer, 1978]

An asymmetry parameter, η, is defined such that $0 \leq \eta \leq 1$

$$\eta = \frac{V_{xx} - V_{yy}}{V_{zz}} .$$

The interaction between the electric quadrupole moment of the nucleus, Q, and the EFG at the nucleus can be represented by the Hamiltonian

$$\hat{H}_Q = \frac{eQV_{zz}}{4I(2I-1)} [3\hat{I}_z^2 - \hat{I}^2 + \eta(\hat{I}_+^2 + \hat{I}_-^2)/2] \qquad (8\text{-}4)$$

where $\hat{I}_z$, $\hat{I}$, and $\hat{I}_\pm$ are nuclear angular momentum operators. The RE site in the pyrochlore structure has a 3-fold symmetry axis therefore $\eta = 0$. Diagonalization of this Hamiltonian yields the eigenvalues E_Q:

$$E_Q = \frac{eQV_{zz}}{4I(2I-1)} [3M_I^2 - I(I+1)] \qquad (8\text{-}5)$$

where M_I is the nuclear magnetic spin quantum number. The result is a splitting of the (2I+1)-fold degenerate states into substates $|I,\pm M_I\rangle$ without shifting the center of the level. Since M_I is squared the EFG cannot separate $\pm M_I$ and some degeneracy remains.

The EFG acting on the nucleus arises from an asymmetry in the surrounding charge distribution. This distribution of charges may be divided into a contribution from valence 4f electrons and another from the surrounding ions, which are

treated as point charges. The principle component of the EFG may be expressed as

$$V_{zz} = (1-\gamma_\infty)(V_{zz})_{lat} + (1-R)(V_{zz})_{val} \qquad (8\text{-}6)$$

The valence electrons interact with the core electrons, distorting them to produce an EFG at the nucleus. This effect shields the nucleus from the full EFG produced by the valence electrons and is accounted for by the (1-R) factor. The distortion of the core electrons by the surrounding point charges is accounted for by $(1-\gamma_\infty)$. These terms are referred to as the Sternheimer shielding parameters [Sternheimer, 1953] although γ_∞ is large and negative [Ingalls, 1962] and is, in fact, an antishielding parameter. For most rare-earth ions the contribution to the EFG by the 4f valence electrons, $(V_{zz})_{val}$, is larger than the contribution from the surrounding lattice [Ofer, 1968]. However, for Gd(+3) and Lu(+3), $(V_{zz})_{val} = 0$ since they are spherically symmetric S-state ions and the only contribution to the EFG is by the surrounding charges.

The valence contribution to the EFG may be expressed as

$$(V_{zz})_{val} = -e\langle J||\alpha||J\rangle\left\langle\frac{1}{r^3}\right\rangle\{\langle 3J_z^2\rangle - J(J+1)\}_T \; . \qquad (8\text{-}7)$$

It is necessary to assume the energy of the first excited multiplet E_J, >> kT, a good assumption for Yb(+3) [Dieke, 1968]. The

reduced matrix elements $\langle J||\alpha||J\rangle$ are tabulated by Hutchings [1964]. The Boltzmann thermal average over crystalline electric field substates is indicated by $\{\ \}_T$.

The lattice contribution to the EFG may be related directly to the crystal field B_2^0 term

$$(V_{zz})_{lat}(1-\gamma_\infty) = \frac{-4B_2^0(1-\gamma_\infty)}{\langle J||\alpha||J\rangle\langle r^2\rangle(1-\sigma_2)} \qquad (8\text{-}8)$$

where $\langle J||\alpha||J\rangle$ and $\langle r^2\rangle$ were discussed in Chapter 6. $(1-\sigma_2)$ represents the shielding of 4f electrons from the outer field 5s and 5p shells [Wallace, 1977].

The nuclear magnetic moment may interact with unpaired electron moments. The Hamiltonian takes the form [Gütlich, 1978]

$$\hat{H}_M = -g_N\mu_N\underline{\hat{I}}\cdot\underline{\hat{H}}_{eff} \qquad (8\text{-}9)$$

where H_{eff} is the effective field felt by the nucleus. This field may be composed of several contributions [Ofer, 1968]

$$\underline{\hat{H}}_{eff} = \underline{\hat{H}}^{4f}_{eff} + \underline{\hat{H}}^{core}_{eff} + \underline{\hat{H}}^{cond}_{eff} + \underline{\hat{H}}^{res}_{eff} \qquad (8\text{-}10)$$

where the last three terms are effective field operators arising from core electrons, conduction electrons and dipolar or external fields. Generally the contribution from the unpaired

4f electrons, $\hat{H}^{4f}_{eff}$, is large enough that the other contributions may be ignored. If J is a good quantum number, the effective field operator may be expressed as

$$\hat{H}^{4f}_{eff} = 2\mu_B \langle 4f|\frac{1}{r^3}|4f\rangle \langle J||N||J\rangle \hat{J} \qquad (8\text{-}11)$$

where $\langle J||N||J\rangle$ is a reduced matrix element, defined by Abragam [1970]. It is in this way that the effective field felt by the nucleus is proportional to the ionic magnetic moment. Meyer et al. [1979] have determined the effective field felt by the nucleus for a free ion. The proportionality

$$\frac{H^{4f}_{eff}}{H_{FI}} = \frac{\langle J_z \rangle}{J} \qquad (8\text{-}12)$$

can then be written, where H_{FI} is the free ion effective field.

The eigenvalues for the magnetic interactions have the form

$$E_{M(M_I)} = -g_N \mu_N H_{eff} M_I \qquad (8\text{-}13)$$

The effect of the magnetic interactions is to split the nuclear state into (2I+1) equally spaced, non degenerate substates $|I,M_I\rangle$.

Many rare earth ions may have both magnetic hyperfine and quadrupolar interactions present simultaneously, and the hyperfine Hamiltonian, Eq. (8-2), may be replaced by

$$\hat{H}_M = - a_0[\hat{I}_z\cos\theta + (\hat{I}_x\cos\phi + \hat{I}_y\sin\phi)\sin\theta]$$

$$\hat{H}_Q = A_0[3\hat{I}_z^2 - \hat{I}^2 + \eta(\hat{I}_x^2-\hat{I}_y^2)] \qquad (8\text{-}14)$$

where θ and ϕ represent the polar and azimuthal angles between the principle axes of the effective field and the EFG. Also

$$a_0 = g_e\mu_N\hat{H}_{eff} \qquad (8\text{-}15)$$

and

$$A_0 = e^2QV_{zz}/[4I_e(2I_e-1)] \; . \qquad (8\text{-}16)$$

g_e, Q_e and I_e represent values for the nuclear excited state since $I = 0$ for the ground state of ^{170}Yb.

The splitting pattern of the nuclear energy levels by a magnetic hyperfine field and an EFG is shown in Fig. 8-1.

The ^{170}Yb Mössbauer spectrum for $Yb_2V_2O_7$ can be used to determine the magnetic moment of Yb(+3) by use of Eqs. (8-11) and (8-12). This moment can then be used in Eq. (8-7) to determine the valence contribution to the EFG and finally, after determining the lattice contribution to the EFG, B_2^0 can be estimated using Eq. (8-8).

Data Treatment

Details of the data collection may be found in Chapter 2. After folding the spectra, they were fitted to various models using the program GMFP. This is a general Mössbauer fitting program designed by Ruebenbauer and Birchall [1979]. It

is generalized to treat arbitrary spins by a full diagonalization of the Hamiltonian. The fitting was done using transmission integrals, although the option for fitting Lorentzian line shapes was available. The option to simulate spectra also proved useful.

Discussion

The ^{170}Yb Mössbauer spectra of $Yb_2V_2O_7$ at 4K and 80K are shown in Figs. 8-1 and 8-2. The refined parameters obtained from these spectra are given in Table 8-2.

The five lines in the 4K spectrum were attributed to a large magnetic hyperfine and a smaller electric quadrupole interaction. The effective field acting on the nucleus was determined, from a_0, to be 1807(7) kOe. The angle between the principle axis of the EFG and the effective field was assumed to be zero. Meyer et al. [1979] reported a ^{170}Yb free ion effective field of 4160(60) kOe based on Mössbauer studies of $YbFe_2$. Calculations reported by Dunlap [1971] are in agreement with this value. A simple ratio of effective fields leads to an experimental electronic moment on Yb(+3) of 1.73(3) μ_B. This result is in excellent agreement with previous determinations from neutron diffraction and saturation magnetization data as well as with crystal field calculations. It supports the previous assumption that the magnetic behaviour of the vanadium atoms remains unchanged across the series $(RE)_2V_2O_7$; RE = Lu, Yb, Tm. The value obtained for the ground state moment

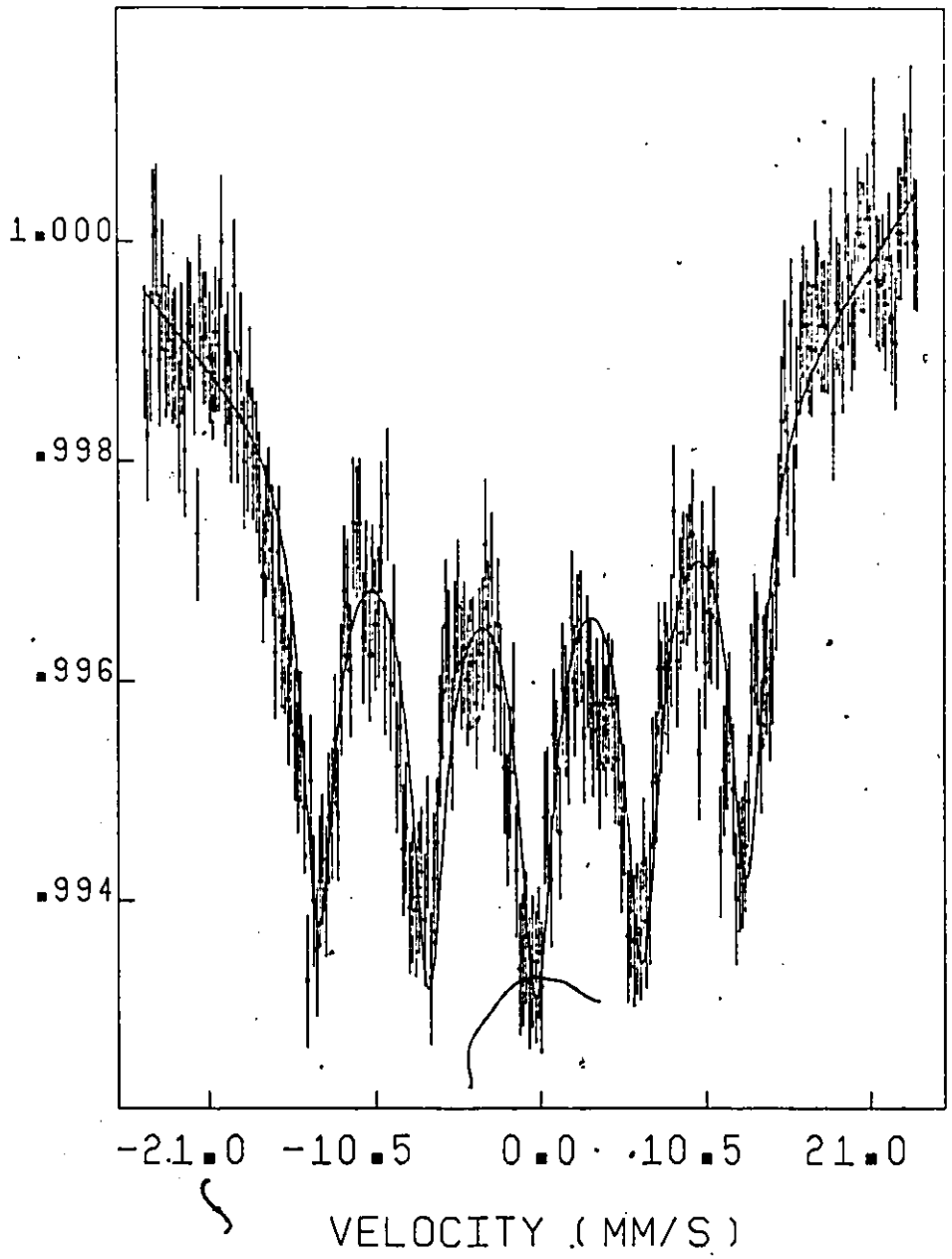

Figure 8-1 ^{170}Yb Mössbauer spectrum of $Yb_2V_2O_7$ taken at 4K.

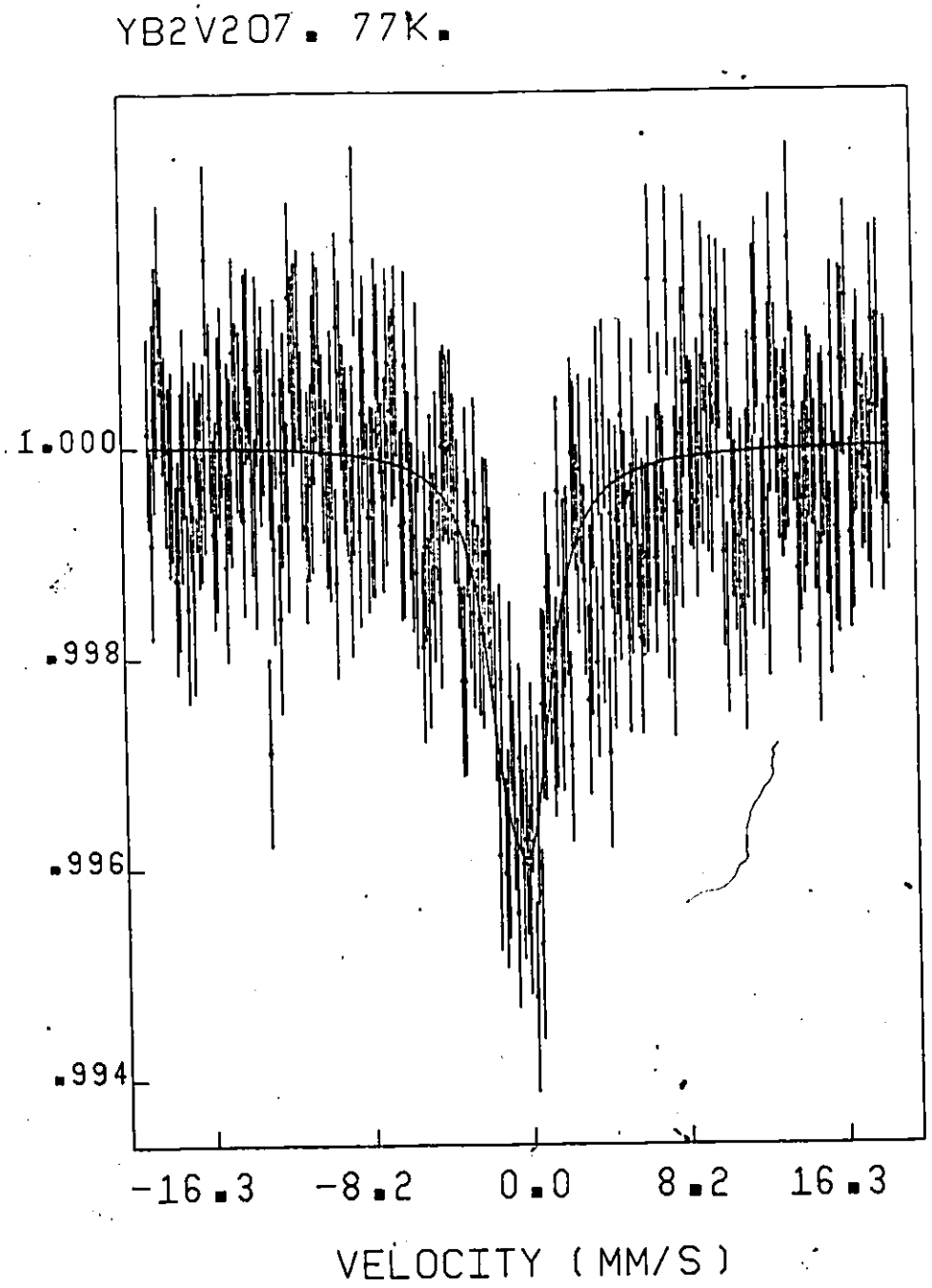

Figure 8-2 ^{170}Yb Mössbauer spectrum of $Yb_2V_2O_7$ taken at 77K.

Table 8-2

^{170}Yb Mössbauer Results on $Yb_2V_3O_7$

	4K(mm sec^{-1})	80K(mm sec^{-1})
recoilless fraction	.212(4)	
sample thickness	.182(2)	
source line width	1.02*	
dispersion correction	-0.03*	
ΔE_M	6.80(3)	0*
$eQV_{zz}/4I(2I-1)$	-.021(7)	-0.14(3)
isomer shift	-.78(3)	-0.78*
sample line width	1.95(3)	1.95*
H_{eff}	1807 kOe	-
$g\langle J\rangle$	1.73(3) μ_B	-
eQV_{zz}	-.50(17) mm sec^{-1}	-3.3(8) mm sec^{-1}

*values fixed in refinement

is also in good agreement with that reported for the isostructural $Yb_2Ti_2O_7$ [Townsend and Crossley, 1968; Dunlap et al., 1978].

Having obtained $\langle J_z \rangle_{4K}$ from the magnetic splitting, it is possible to calculate

$$eQ(V_{zz})_{val}(1-R) = -e^2\langle J||\alpha||J\rangle \langle r^{-3}\rangle\{\langle 3J_z^2\rangle - J(J+1)\}_{4K} .$$

Using $\langle J||\alpha||\rangle = \frac{2}{63}$ [Hutchings, 1964], $\langle r^{-3}\rangle = 12.6\ a_0^{-3}$ [Judd, 1963, $J = \frac{7}{2}$ and $\langle J_z\rangle = 1.51$, the valence contribution to the splitting of the Mössbauer lines was determined to be -19.5 mm sec^{-1}. The experimental splitting is -1.5 mm sec^{-1} therefore, using Eq. (8-6), the lattice contribution was determined as +18 mm sec^{-1}. B_2^0 was then calculated using Eq. (8-8), estimating the value of $(1-\gamma_\infty)/(1-\sigma_2) = 200$ [Dunlap, 1978], and found to be 19(7) K.

The lattice contribution to the EFG calculated here is larger than expected. Mössbauer spectroscopy on an isostructural series of gadolinium compounds was used to measure $(V_{zz})_{lat}$ directly, since $(V_{zz})_{val} = 0$ for an S-state ion. Values of the lattice contribution, along with oxygen x-parameters, for these compounds are listed in Table 8-3. Recalling, from Chapter 3, that the higher the x-parameter the more distorted is the rare-earth environment from cubic symmetry, the expected quadrupole splitting based on the gadolinium data [Calage and Pannetier, 1977] is about 10.5 mm sec^{-1} for $Yb_2V_2O_7$. This corresponds to a B_{12}^0 of 12 K. There appears to be a discrepancy between the B_2^0 terms calcula-

ted using data for $Gd_2Ru_2O_7$ and $Yb_2V_2O_7$. It is felt that the valence contribution to the EFG should be known well since $\langle J_z \rangle_{4K}$ has been determined by several different techniques. It should be pointed out that the error in eQV_{zz} is large, probably resulting from the high correlation of the EFG and the line width. However, it was shown in the previous chapter that the magnetic behaviour appears insensitive to a B_2^0 in the range $0K < B_2^0 < 14K$. While B_2^0 may be slightly larger than 14K, there is no reason to assume this will greatly alter the energy level scheme proposed based on crystal field calculations.

The spectrum obtained at 80K was a broad, single line. Since the critical temperature for $Yb_2V_2O_7$ is 73.2(5)K, ΔE_M was assumed to be zero. The linewidth used to fit the spectrum was fixed at the value obtained from the 4K spectrum, and the quadrupole splitting was determined to be 3.3(8) mm sec^{-1}. Unfortunately, because of the assumptions necessary to obtain this value, and the relatively poor statistics on the 80K spectrum, the quadrupole splitting was assumed to be less reliable than that of the 4K spectrum. However, it should be pointed out that the B_2^0 term obtained from these data is 11K, consistent with results from $Gd_2Ru_2O_7$.

The ^{170}Yb Mössbauer spectra have confirmed an atomic moment on Yb(+3) of 1.73(3) μ_B. This is the only technique used which gives an estimate of the moment independent of the

Table 8-3

Quadrupole Splitting and Oxygen x-parameters for Several Gd Compounds [Calage and Pennetier, 1977]

	x (48f)	$eQV_{zz}(1-\gamma_\infty)$*	$eQV_{zz}(1-\gamma_\infty)$**
Gd_2TiO_7	.428	-11.37	15.30
$Gd_2Ru_2O_7$	.422	-8.08	10.87
$Gd_2Sn_2O_7$	.418	-7.86	10.58

* ^{155}Gd 87 keV transition

** ^{170}Yb corrected $Q_{Yb}/Q_{Gd} = -1.35$ and assuming $(1-\gamma_\infty)_{Yb} = (1-\gamma_\infty)_{Gd}$. This assumption has been supported experimentally [Ofer, 1968].

moment of the vanadium atoms and that the moment is reduced from the free ion value of 4.0 μ_B. Low saturation moments on Yb(+3) are not unusual. There are several reports in the literature of compounds containing this ion, in various environments, with ground state moments of about 2.0 μ_B, some examples of which are shown in Table 8-4.

Table 8-4

Some Compounds with Reduced Yb(+3) Saturation Moments

Compound	μ_{sat}	Determined by	Site Symmetry	
$YbAlO_3$	2.49(5)	Mössbauer	2	Bonville et al., 1978
Yb in YGG	1.71	CEF calc.	222	Hutchings and Wolf, 1964
$YbTiO_3$	1.85(10)	Mössbauer	2	Soderholm, unpubl.
Yb_2TiO_3	1.91(8)	Neutron diffraction	2	Moon, 1968
$YbMo_6S_8$	1.70	Mössbauer	$\bar{3}$	Bonville et al., 1980
$YbAl_3$	1.89	Mössbauer	32	Ross and Tronc, 1978
$Yb_2Ti_2O_7$	1.71	CEF calc/Mössbauer	$\bar{3}$m	Dunlap et al., 1978
$Yb_3Fe_5O_{12}$	1.7	Magnetization	222	Guillot and Pauthenat, 1964
$Cs_2NaYbCl_6$	1.7	CEF calc.	m3m	Dunlap and Shenoy, 1975

CHAPTER 9

CONCLUSIONS

The pyrochlores $(RE)_2V_2O_7$; RE = Lu, Yb, Tm, have been treated as systems of two interpenetrating magnetic sublattices, one of vanadium and the other rare-earth ions. The simplest of these compounds is $Lu_2V_2O_7$, since Lu(+3) is diamagnetic. The magnetic data for this compound are consistent with ferromagnetic ordering of the vanadium spins below 74K, in agreement with previous reports (Bazuev et al., 1976; Shin-ike et al., 1977; Bazuev et al., 1978a]. The vanadium atoms are too far apart for direct exchange but structural data were used to argue that a super exchange pathway, involving an intermediary oxygen atom, is probably involved in the cooperative effects.

The magnetic behaviour of the vanadium sublattice appears independent of the moment on the rare-earth atom. The vanadium-vanadium exchange is the dominant interaction, and is responsible for the magnetic ordering, at about 70K, for all three pyrochlores. While there is no evidence to suggest that the rare-earth sublattices in both $Yb_2V_2O_7$ and $Tm_2V_2O_7$ do not remain paramagnetic down to 4K, the vanadium atoms do create a weak exchange field, which is felt by the rare earth moments, and causes a net magnetization which is parallel to that of

the vanadium sublattice. This parallel alignment is in contradiction to the arguments used to predict the exchange coupling of rare earth moments in the iron garnets [Gilleo, 1980]. These arguments predicted that the RE-V coupling in the pyrochlores should be antiparallel. The relative weakness of the rare-earth-vanadium exchange has been accounted for by the spatial isolation of the RE atoms in the pyrochlore structure.

The low saturation moments for $Yb_2V_2O_7$ and $Tm_2V_2O_7$ were accounted for by crystal field quenching of the total moment. Calculated susceptibilities, assuming a cubic crystalline electric field, were found to agree well with the experimentally determined behaviour of the rare-earths in these compounds. The temperature independence of the Tm(+3) sublattice susceptibility at very low temperatures, with a change to temperature dependent behaviour at about 140K was explained by a ground state singlet with a low lying excited state. The ground state moment of Yb(+3) was calculated to be 1.71 μ_B, in excellent agreement with the value obtained from neutron diffraction, Mössbauer, and saturation magnetization data. There have been other compounds in the literature which have Yb(+3) moments much lower than the expected free ion value of 4.0 μ_B. Some of these compounds are listed in Table 8-4.

The large energy difference, 1100K, between the ground and first excited states in Yb(+3) makes the calculated moment relatively insensitive to deviations from cubic symmetry. The crystal field parameters, and the value of the ground state

moment, for Yb(+3) in $Yb_2V_2O_7$, agree well with values obtained for the isostructural compound $Yb_2Ti_2O_7$ [Townsend and Crossley, 1968]. However a comparison of B_2^0 terms, obtained for these two compounds from ^{170}Yb Mössbauer data, shows there to be significantly less axial distortion in the case of the titanium pyrochlore (see Chapter 8).

It now appears that the magnetic properties of the vanadium pyrochlores are fairly well understood and these materials are indeed members of the unusual class of ferromagnetic oxides. While these compounds have been determined to be ferromagnetic, little has been said about their electrical properties, although they have been reported to be semiconductors [Bazuev et al., 1976; Shin-ike et al., 1977]. As previously suggested [Soderholm and Greedan, 1979b], electrical conductivity in oxides of the type studied here is often attributed to a small polaron hopping mechanism. Hall effect measurements may provide the information necessary to understand the conductivity mechanism. Unfortunately a detailed investigation would require single crystals of these compounds, and, although several attempts were made to find a successful method of crystal growth, more work in this area is needed.

There has been a recent report in the literature that the series $A_2B_2O_7$ (A = Tl, Y; B = Cr, Mn) have been synthesized and all except $Y_2Cr_2O_7$ have the pyrochlore structure [Fujinaka et al., 1979]. Furthermore, a preliminary investigation has

indicated that $Tl_2Mn_2O_7$ is a ferromagnetic semiconductor, with a critical temperature of 117K [Fujinaka et al., 1980] while the others are reported to have high resistivities ($\sim 10^8\ \Omega$ cm). This is very interesting in light of the work done here. A more detailed investigation of these new magnetic pyrochlores may add a further understanding to the behaviour of the class of compounds which are simultaneously ferromagnetic and semiconducting.

REFERENCES

A. Abragam and B. Bleaney, Electron Paramagnetic Resonance of Transition Ions, Clarendon Press, 1970.

A. Arrot, Phys. Rev. 108,:1394 (1957).

N.W. Ashcroft and N.D. Mermin, Solid State Physics, Holt Rinehart and Winston, 1976.

G.E. Bacon, Neutron Diffraction, 3rd edition, Clarendon Press, 1975.

G.E. Bacon, Neutron Scattering in Chemistry, Butterworth and Co., 1977.

G.V. Bazuev, O.V. Makorova, V.Z. Oboldin and G.P. Shveikin, Akad. Nauk. SSSR 230:869 (1976).

G.V. Bazuev, A.A. Samokhvalov, Y.N. Morozov, I.I. Matveenko, V.S. Babushkin, T.I. Arbuzova and G.V. Shveikin, Sov. Phys. Solid State 19:1913 (1978a).

G.V. Bazuev and G.P. Shveikin, Izv. Akad. Nauk. SSSR, Neorg. Mater. 14:267 (1978b).

F. Bertaut and F. Forrat, Compt. Rend. 242:382 (1956).

F. Bertaut and R. Pauthenet, Proc. Inst. Elect. Eng. B104:261 (1957).

P. Bonville, J.A. Hodges and P. Imbert, Phys. Rev. B, 18(5):2196 (1978).

P. Bonville, J.A. Hodges, G. Jehanno, R. Chevral and M. Sargent, Revue Phys. Appl. 15:1139 (1980).

E.A. Boudreaux and L.N. Mulay, Theory and Application of Molecular Paramagnetism, John-Wiley and Sons, 1976.

W. Bragg, Proc. Roy. Soc. A89:468 (1914).

W.F. Brown, Phys. Rev. 60:139 (1941).

M.J. Buerger, Crystal Structure Analysis, J. Wiley & Sons, 1960.

Y. Calage and J. Pannetier, J. Phys. Chem. Solids 38:711 (1977).

A. Casalot and P. Hagenmuller, J. Phys. Chem. Solids 30:1341 (1969).

C.A. Catanese, A.T. Skjeltorp, H.E. Meissner and W.P. Wolf, Phys. Rev. B 8(9):4223 (1973).

J. Crangle and G.M. Goodman, Proc. Roy. Soc. London Ser A321:477 (1971).

B.D. Cullity, Introduction to Magnetic Materials, Addison-Wesley, 1972.

G.H. Dieke, Spectra and Energy Levels of Rare Earth Ions in Crystals, Interscience 1968.

B.D. Dunlap, Mössbauer Effect Methodology, ed. I.J. Gruverman, Plenum Press 7:123 (1971).

B.D. Dunlap and G.K. Shenoy, Phys. Rev. B12(7):2716 (1975).

B.D. Dunlap, G.K. Shenoy, J.M. Friedt, M. Meyer and G.J. McCarthy, Phys. Rev.B18:1936 (1978).

W.A. Fertig, D.C. Johnson, L.E. Delong, R.W. McCallum, M.B. Maple and B.T. Matthias, Phys. Rev. Lett. 38(17):987 (1977).

A.J. Freeman and R.E. Watson, Acta Cryst. 14:27 (1961).

A.J. Freeman and R.E. Watson, Phys. Rev. 127:2050 (1962).

H. Fujinaka, N. Kinomura, M. Koizum, Mat. Res. Bull. 14:1133 (1979).

H. Fujinaka, N. Kinomura, Y. Miyamoto, S. Kume and M. Koizumi, High Pressure Science and Technology, Proceedings of the VIIth International AIRAPT Conf. Pt. 1, Pergamon, 1980, p. 556.

F.S. Galasso, Structure + Properties of Inorganic Solids, Pergamon Press 1970.

J. Galy, J. Darriet, A. Casalot and J.B. Goodenough, JSS Chem. 1:339 (1970).

J.D. Garrett, J.E. Greedan, D.A. MacLean, Mat. Res. Bull. 16:145 (1981) and references therein.

S. Geller and M.A. Gilleo, J. Phys. Chem. Solids 3:30 (1957).

S. Geller and M.A. Gilleo, J. Phys. Chem. Solids 9:235 (1959).

M.A. Gilleo, Ferromagnetic Materials, Vol. 2, ed. E.P. Wohlfarth North-Holland Publishing 1980.

J.B. Goodenough, Czech. J. Phys. B17:304 (1967).

J.P. Goral and J.E. Greedan, unpublished neutron diffraction data.

J.E. Greedan, Mat. Res. Bull. 14,13 (1979).

M. Guillot, R. Pauthenat, Compt. Rend. 259:1303 (1964).

P. Gütlich, R. Link and A. Trautwein, Mössbauer Spectroscopy and Transition Metal Chemistry, Springer-Verlag 1978.

W. Heisenberg, Z. Physik, 38:411 (1926).

W. Heisenberg, Z. Physik, 49, 619 (1928).

H. L'Helgoualch, G. Fonteneau and J. Pannetier, "MARYSE", Powder structure refinement program. Unpublished (1975).

L.M. Holmes, T. Johansson and H.J. Guggenheim, Solid State Comm. 12:993 (1973).

R.M. Hornreich, J. Mag. Mat. 7:280 (1978) and references therein.

R.M. Hornreich, B.M. Wanklyn and I. Yaeger, Int. J. Mag. 2:77 (1972).

M.T. Hutchings, Solid State Physics 16:227 (1964).

M.T. Hutchings and W.P. Wolf, J. Chem. Phys. 41(3):617 (1964).

R. Ingalls, Phys. Rev. 128:1155 (1962).

D. Johnston, Ph.D. Thesis, University of California, San Diego, 1975.

T. Jones, L.R. Norlock, and R.R. Boucher, J. Less Common Metals 5:128 (1963).

V.M. Judin and A.B. Sherman, Solid State Commun. 4:661 (1966).

J. S. Kasper and K. Lonsdale, ed, International Tables for X-ray Crystallography II:291 (1959).

O. Knop, F. Brisse and L. Castelliz, Can. J. Chem. 43:2812 (1965).

O. Knop and F. Brisse, Can. J. Chem. 46:859 (1968).

O. Knop F. Brisse and L. Castillez, Can. J. Chem. 47:971 (1969).

K.R. Lea, M.J.M. Leask and W.P. Wolf, J. Phys. Chem. Solids 23:1381 (1962).

C.M. Lederer and V.S. Shirley, ed., Table of Isotopes, John Wiley and Sons, 1978, 7th edition.

H.W. Lehmann, Phys. Rev. 163(2):488 (1967).

I.N. Levine, Quantum Chemistry, Allyn and Bacon Inc., 1974.

D. Lorin, J.M. Dance, J.L. Soubeyroux, A. Tressaud and P. Hagenmuller, J. Magn. and Magn. Mat. 23(1):92 (1981).

R.E. Mabbs abd D.J. Machin, Magnetism and Transition Metal Complexes, Chapman and Hall 1973.

J.B. MacChesney, R.C. Sherwood and J.F. Potter, J. Chem. Phys. 43:1907 (1965).

D.A. MacLean, H-N Ng and J.E. Greedan, J. Solid State Chem. 30:35 (1979).

R.L. Martin, New Pathways in Inorganic Chemistry, Cambridge Press 1968.

B.T. Matthias, R.M. Bozorth, J.H. Van Vleck, Phys. Rev. Lett. 7(5):160 (1961).

R.A. McCauley, J. Appl. Phys. 51(1):290 (1980).

T.R. McGuire, B.E. Argyle, M.W. Shafer and J.S. Smart, Appl. Phys. Lett. 1:17 (1962).

T.R. McGuire and P.J. Flanders, Magnetism and Metallurgy, ed. A.E. Berkowitz and E. Kneller, pp. 124-189, Academic Press 1969.

T.R. McGuire and M.W. Shafer, J. Appl. Phys. 35:984 (1964).

C. Meyer, Y. Gros, F. Hartmann-Boutron and J.J. Capponi, J. de Phys. 40:403 (1979).

A. Michel, G. Chaudron and J. Bénard, J. Phys. Rad. 12:189 (1951).

R.M. Moon, Phys. Rev. 176:722 (1968).

A.H. Morrish, The Physical Principles of Magnetism, New York: J. Wiley and Sons, 1966, pp. 680.

L.G. Nikiforov, Soviet Physics - Crystallography, 17(2):347 (1972).

S. Ofer, I. Nowik and S.G. Cohen, Chemical Applications of Mössbauer Spectroscopy, ed. V.I. Goldanskii and R.H. Herber, Academic Press 1968, pp. 427-501.

M.G. Paton and E.N. Malsen, Acta Cryst. 19:307 (1965).

J.J. Pearson, G.F. Hermann, K.A. Wickersheim, R.A. Buchanan, Phys. Rev. 159(2):251 (1967).

A.F. Reid and M.S. Sienko, Inorg. Chem. 6(3):521 (1967).

J.W. Ross and E. Tronc, J. Phys. F: Metal Physics 8(5):983 (1978).

J.M. Rowe, Ph.D. Thesis, McMaster University, Hamilton, Ont. 1966.

K. Ruebenbauer and T. Birchall, Hyperfine Interactions 7:125 (1979).

M. Sachs, Solid State Theory, McGraw-Hill, 1963.

R.D. Shannon, Acta Cryst. A32:751 (1976).

T. Shin-ike, G. Adachi and J. Shiokawa, Mat. Res. Bull. 12:1149 (1977).

G. Shirane, Acta Cryst. 12:282 (1959).

K.P. Sinha and N. Kumar, Interactions in Magnetically Ordered Solids, Oxford University Press 1980.

J.S. Smart, Effective Field Theories of Magnetism, Philadelphia: W. B. Saunders 1966.

L. Soderholm and J.E. Greedan, Rare Earths Science and Technology: Vol. 2, ed. J.J. Rhyne, Plenum Press p. 392 (1979a).

L. Soderholm and J.E. Greedan, Mat. Rest. Bull. 14:1449 (1979b).

L. Soderholm , J.E. Greedan and M.F. Collins, J. Solid State Chem. 35:385 (1980).

L. Soderholm, C.V. Stager and J.E. Greedan, J. Solid State Chem. 43: 175 (1982).

L. Soderholm and J.E. Greedan, Mat. Res. Bull. 17:707 (1982).

G.L. Squires, Introduction to the Theory of Thermal Neutron Scattering, Cambridge University Press, 1978.

H.E. Stanley, Introduction to Phase Transitions and Critical Phenomena, Oxford University Press, 1971.

C. Stassis, W.H. Deckman, B.N. Harmon, J.P. Desclaux and A.J. Freeman, Phys. Rev. B15:369 (1977).

R.M. Sternheimer, Phys. Rev. 93:1460 (1953).

K.W.H. Stevens, Proc. Roy. Soc. London A1952:209 (1952).

M.G. Townsend and W.A. Crossley, J. Phys. Chem. Solids 29:593 (1968).

K.N.R. Taylor and M.I. Darby, Physics of Rare Earth Solids, Chapman and Hall Ltd. 1972.

I. Tsubokawa, J. Phys. Soc. Japan, 15:1664 (1960).

C.W. Turner, Ph.D. Thesis, McMaster University (1982).

C.W. Turner, M. F. Collins and J.E. Greedan, J. Magn. and Magn. Mat. 23:265 (1981) and references therein.

J.H. Van Vleck, The Theory of Electric and Magnetic Susceptibilities, Oxford University Press 1932.

W.E. Wallace, S.G. Sankar, V.U.S. Rao, Structure and Bonding, 33:1 (1977).

P. Weiss, J. Phys. Radium 6:667 (1907).

W.P. Wolf, M.J.M. Leask, B. Mangum and A.F.G. Watt, J. Phys. Soc. Japan, Suppl, 17:487 (1961).

H.S. Yamada, J. Phys. Soc. Japan 37:667 (1974).